Experimental Evaluation and Mathematical Modeling of the Pharmacokinetics of Boronophenylalanine-Fructose (BPA-f) in Murine Tumor Models

by

Cynthia Fu-Yu Chuang

B.S. Electrical Engineering, M.I.T., 1990
M.S. Bioengineering, University of Pennsylvania, 1992
M.S. Nuclear Engineering, M.I.T., 1994

SUBMITTED TO THE DEPARTMENT OF NUCLEAR ENGINEERING IN PARTIAL FULFILLMENT OF THE REQUIREMENTS FOR THE DEGREE OF

DOCTOR OF PHILOSOPHY IN RADIOLOGICAL SCIENCES

at the
MASSACHUSETTS INSTITUTE OF TECHNOLOGY
June 1999

Signature of Author: _____
Department of Nuclear Engineering, May 18, 1999

Certified by: _____
Dr. Robert G. Zamenhof, Thesis Supervisor
Associate Professor of Radiology, Harvard Medical School

_____
Dr. Paul M. Busse, Thesis Supervisor
Assistant Professor of Radiation Oncology, Harvard Medical School

_____
Prof. Jacquelyn C. Yanch, Thesis Reader
Associate Professor of Nuclear Engineering and
Whitaker College of health Sciences and Technology

Accepted by: _____
Prof. Sow-Hsin Chen
Chairman, Department Committee on Graduate Students

Experimental Evaluation and Mathematical Modeling of the Pharmacokinetics of Boronophenylalanine-Fructose (BPA-f) in Murine Tumor Models

by

Cynthia Fu-Yu Chuang

Submitted to the Department of Nuclear Engineering on May 14, 1999
in Partial Fulfillment of the Requirements for the Degree of

Doctor of Philosophy in Radiological Sciences

ABSTRACT

With the completion of the fission converter epithermal neutron beam (FCB) at MIT, which has a higher epithermal neutron flux (1.3 x 10^{10} neutrons/cm^2sec) than the current m-67 beam, future BNCT irradiations conducted by the Harvard-MIT BNCT program could be reduced from approximately 3 hours per beam to just a few minutes. Therefore, it is essential to determine the optimal time after BPA administration to deliver the neutron irradiation, thereby maximizing the dose to tumor and minimizing the dose to the normal tissues.

The major goal of this thesis was to gain detailed knowledge of the temporal and spatial distribution of ^{10}B in normal tissues and tumors following intravenous BPA-fructose administration, and to use a three-compartment model to study the pharmacokinetics of BPA-f in these tissues. This entailed the investigation of the time-dependent biodistribution of BPA-f in normal brain and in two murine tumor models, GL261 glioma and intracranial B16 melanoma.

From the normal brain study it was shown that there were slight variations in the spatial BPA-f biodistribution in normal brain tissues. The cerebellum and the intracranial nerves consistently showed higher ^{10}B concentrations than the right cerebrum, the left cerebrum, and the brainstem throughout the whole time course studied. This result, if verified, has important treatment planning implications.

It was observed that for GL261 glioma tumor, both the tumor to normal brain ratio and the tumor to blood ratio varied with time, and the best time for neutron irradiation was probably around 60 minutes after the bolus injection. For the B16 intracranial melanoma murine model, the neutron irradiation could be performed during the time frame between 60 and 80 minutes after the bolus injection. The three-compartment pharmacokinetic model parameters (k1 through k4) for GL261 tumor were 0.14 ml/g/min, 0.12 min^{-1}, 0.08 min^{-1}, and 0.036 min^{-1}, respectively, and

for B16 tumor were 0.22 ml/g/min, 0.19 min^{-1}, 0.058 min^{-1}, and 0.011 min^{-1}. The rate constants from the murine tumor models differed substantially from the values another investigator (Imahori) obtained for human GBM by PET scanning, which were 0.027 ml/g/min, 0.041 min^{-1}, 0.029 min^{-1}, and 0.013 min^{-1}, respectively. From these two intracranial murine tumor models it was shown that both the tumor to blood and tumor to normal brain ^{10}B concentration ratio changed in time, and that the tumor BPA-f pharmacokinetics varied with tumor cell lines, thereby affecting the optimal timing of the irradiation.

An additional experiment was conducted to investigate whether hepatic colorectal metastasis, another tumor refractory to current treatments, could be a viable candidate for BNCT. The experiments showed that the tumor boron was up to 2 times higher than in normal liver at 60 and 120 min after the bolus injection. Therefore, even in a highly vascularized host environment such as the liver, there was still preferential uptake of BPA-f by tumor cells, suggesting that colorectal liver metastases might be a suitable opportunity for BNCT.

Our results show that the animal models we have studied are associated with highly complex BPA pharmacokinetics. This reveals practical treatment planning concerns with regard to radiation sensitive areas such as the optic chiasm due to the higher ^{10}B concentrations observed in the intracranial nerves. Our results also demonstrate different BPA pharmacokinetics in different tumor lines. Therefore, although a three-compartment model can be used to study the pharmacokinetics, a uniform set of pharmacokinetics parameters cannot be used. Our results further show that although the uptake ratio in hepatic colorectal metastasis might not be sufficient for BNCT, preferential uptake is still demonstrated in a highly vascularized host environment, an indication that other tumors might be plausible candidates for BNCT.

Thesis Supervisor: Robert G. Zamenhof
Title: Associate Professor of Radiology at Harvard Medical School

Thesis Supervisor: Paul M. Busse
Title: Assistant Professor of Radiation Oncology at Harvard Medical School

Acknowledgments

It would be difficult for me to express my gratitude to Dr. Robert Zamenhof for giving me the opportunity to work on this thesis project. It has been a rewarding experience to work with and learn from an expert in BNCT who is never short of new and clever ideas. I would like to express my heartfelt thanks to Dr. Paul Busse for helping me develop my experimental skills over the past few years. He has always been helpful in offering suggestions and insights in the radiobiological aspects of my thesis work whenever I needed them.

I want to thank Professor Jacquelyn Yanch for being my thesis reader and giving me valuable constructive suggestions, and for always being very supportive and encouraging. The modeling work in my research would have been much more difficult if not for the suggestions of Dr. Matthew Palmer, whose help and guidance were much appreciated. I would also like to thank Professor Otto Harling for his insightful comments and suggestions on many aspects of my thesis work. I would like to express my sincere thanks to Dr. Jeff Coderre for serving on my committee, and for providing expert advice on the radiobiology of BNCT. I am also grateful to Dr. John Bernard for all his help and encouragement throughout the years.

I want to thank everyone in the BNCT group for making it a good place to work. I especially thank Stead Kiger for his helpful ideas on improving the quality of my research, and the numerous discussions we had ranging from data analysis, programming to dose calculation were invaluable. A special thanks to Kent Riley for his instructions in the usage of PGNAA and ICP-AES facilities, his help in maintaining the hardware, and his patience in answering my endless questions. Tim Goorley's sunny disposition and the stimulating conversations we had in the lab often helped to relieve the stress and frustrations I experienced this past year, and I especially appreciate his help in running MCNP for the optic nerve dose calculations. I am extremely grateful to Jody Kaplan for her endless patience, her willingness to listen and her unlimited support. I am especially grateful for the time she spent in reading my thesis and correcting my English. I thank Dr. Lujia Tang for her help and advice on cell culture work and for taking care of all the administrative work in the lab, without her, the lab might not have run as smoothly.

I would like to thank the people in Reactor Operations for their support in my seemingly endless hours of work at the 4DH3 beam facility. I would especially like to thank the following people: Eddie Lau and Tom Newton for their patient accommodation in scheduling the use of the reactor; and Frank Warmsley for all his help in conducting irradiations at the 2PH2 beam, and ordering the Argon gas tanks for the ICP-AES equipment and the CO_2 for dry ice. Of course, I would like to express my sincere thanks to Carolyn Medeiros and Kathy O'Connel for lending their sympathetic ears.

I would also like to thank the Reactor Radiation Protection Office personnel for their support and assistance. I would especially like to thank Fred McWilliams for his patience in answering my numerous questions, and Todd Date for being ever so tolerant when I forgot to turn in my dosimeter readings.

A very special thank goes to Peggy Micca from BNL for her technical assistance on tissue boron quantification technique. I would also like to thank David Northey from Dana Farber Cancer Institute for the instructions in tail-vein injection and intracranial implantation, and continuing help in handling mice. I would also like to acknowledge Bill Dahlberg from Harvard School of Public Health for his expert advice on cell culture work. I also want to thank Dr. Peter Thomas from the Department of Cancer Biology, Beth Israel Deaconess Medical Center for his instruction and the use of his lab during my research on the hepatic colorectal metastasis. Finally, I would like to thank Dr. Osman Cay from the Department of Radiology, Beth Israel Deaconess Medical Center for his preliminary hepatic colorectal metastases research that led to the work done in this thesis.

Finally, I would like to say that I truly thank my parents, my grandmother and my aunt Esther for their unconditional love and support, and special thanks to Madame Lin for her spiritual guidance and advice. Without them, I don't think I would have the strength and courage to continue with my education during the difficult times in the past few years. I would also like to thank my siblings Sandy, David and Yvonne for their love, support and understanding in listening to my complaints throughout the years. I especially thank Sandy for her understanding in my missing her wedding this past April because of my thesis work. It is to my family that this thesis is gratefully dedicated.

This research was supported by the U.S. Department of Energy under Grant No. DE-FG02-97ER62193.

Table of Contents

Abstract 2

Acknowledgments 4

Table of contents 6

List of Figures 8

List of Tables 10

1. Introduction 11

1.1 Background on Boron Neutron Capture Therapy 11

2.2 Research Goals 13

2.3 References 17

2. Analytical Tools 21

2.1 ^{10}B Quantification 21

2.1.1 Introduction 21

2.1.2 PGNAA Method 22

2.1.3 ICP-AES Method 23

2.1.4 Error Analysis 25

2.1.5 Intercomparisons of PGNAA and ICP-AES Measurements of ^{10}B Concentrations in Murine Lungs 26

2.2 Pharmacokinetic Modeling 30

2.2.1 Introduction and Background 30

2.2.2 History of Compartment Modeling in Biological Systems 32

2.3.3 A Two-Compartment Closed System Analysis of Tracer Study 33

2.2.4 Three-Compartment Modeling 36

2.3 References 40

2. Pharmacokinetics of BPA-f in Murine Normal Brain and Tumor Models 42

3.1 BPA-f Pharmacokinetics Study in Normal Murine Brain Tissues **42**
3.1.1 Introduction **42**
3.1.2 Materials and Methods **43**
3.1.3 Results and Discussion **44**
3.2 BPA-f Pharmacokinetics study in An Intracranial Murine GL261 Glioma **52**
3.2.1 Introduction **52**
3.2.2 Materials and Methods **53**
3.2.3 Results and Discussion **56**
3.3 BPA-f Pharmacokinetics Study in B16 Melanoma Bearing Murine Brains **61**
3.3.1 Introduction **61**
3.3.2 Materials and Methods **61**
3.3.3 Results and Discussion **62**
3.4 BPA-f Pharmacokinetics Study in CX-1 Hepatic Colorectal Metastasis **70**
3.4.1 Background **70**
3.4.2 Materials and Methods **71**
3.4.3 Results and Discussion **72**
3.5 Lung ^{10}B Measurements **77**
3.6 References **81**

4. Conclusions and Recommendations for Future Work **84**
4.1 Conclusions and Discussion **84**
4.2 Recommendations for Future Work **88**
4.3 References **92**

List of Figures

Chapter 1	**Introduction**	
Figure 1.1	Nuclear Reactions Of ^{10}B And Thermal Neutrons	12
Chapter 2	**Analytical Tools**	
Figure 2.1	Decay Scheme Of $^{11}B^*$	22
Figure 2.2	Two-Compartment Model	33
Figure 2.3	Diagram Of A Three-Compartment Model for $^{18}FBPA$-f Pharmacokinetics	37
Chapter 3	**Pharmacokinetics of BPA-f in Murine Normal Brain and Tumor Models**	
Figure 3.1	Temporal ^{10}B Concentrations In Blood Following either 250 or 350 mg/kg Bolus Tail Vein Injection of BPA-f	45
Figure 3.2	Temporal ^{10}B Concentrations in Blood and Various Bran Tissues	47
Figure 3.3	Isodose Contours of Optic Chiasm and Normal Brain Under FCB Irradiation	48
Figure 3.4	Temporal Blood and Normal Brain ^{10}B Concentrations with 250 mg/kg Dose Scaled to 350 mg/kg	49
Figure 3.5	Predicted and Experimental Normal Brain ^{10}B Concentrations	50
Figure 3.6	A Mouse with Hunched Back, Typical Sign of Intracranial Tumor	56
Figure 3.7	Temporal ^{10}B Concentrations in Blood, Normal Brain and GL261	57
Figure 3.8	^{10}B concentration Ratio between Blood, Brain and GL261 Tumors	58
Figure 3.9	Experimental and 3-Compartment Fitted Data for GL261	59
Figure 3.10	H & E Stained Sections of Normal Murine Brain	60
Figure 3.11	H & E Stained Section of GL261 Tumor	60
Figure 3.12	Murine Brain with B16 Intracranial Melanoma	63
Figure 3.13	Intracranial Gl261 Tumor1	63
Figure 3.14	Temporal ^{10}B Concentrations in Blood, Normal Brain, Intracranial B16, Subcutaneous B16 and Skin	66

Figure 3.15 ^{10}B Concentration Ratios between Blood, Brain, Intracranial B16 67
Figure 3.16 Experimental and 3-Compartment Fitted Data for B16 68
Figure 3.17 3-Compartment Predicted Ratio for GL261, Blood and Normal Brain 69
Figure 3.18 3-Compartment Predicted Ratio for B16, Blood and Normal Brain 69
Figure 3.19 Temporal ^{10}B Concentrations in Blood, Normal Liver, and Hepatic Colorectal Metastases 73
Figure 3.20 Temporal ^{10}B Concentration Ratio between Blood, Liver, Hepatic Colorectal Metastases and Skin 74
Figure 3.21 Liver Dose Rate Profile from Rission Converter Beam 75
Figure 3.22 H & E Stained Section of Normal Liver 76
Figure 3.23 H & E Stained Section of Hepatic Colorectal Metastases 76
Figure 3.24 Temporal ^{10}B Concentrations in Blood, Normal Brain, and Lungs 78

Chapter 4 Conclusions and Recommendations for Future Work

Figure 4.1 Predicted ^{10}B concentration ratio between B16/blood, B16/normal brain, and normal brain/blood 86

List of Tables

Chapter 2	**Analytical Tools**	
Table 2.1	PGNAA Repeatibility test	27
Table 2.2	PGNAA Measurements of Small Lung Tissues	28
Table 2.3	Intercomparison of PGNAA and ICP-AES ^{10}B Measurements in Lung Tissues	29
Chapter 3	**Pharmacokinetics of BPA-f in Murine Normal Brain and Tumor Models**	
Table 3.1	k1 through k4 Pharmacokinetics Parameters for GL261, B16 and GBM	65
Table 3.2	PGNAA Measurements of Lung Tissues	79

Chapter 1

Introduction

1.1 Background

Boron neutron capture therapy (BNCT) is a binary radiation therapy modality that has the potential to selectively target tumor cells[1-3]. The physical principle of BNCT was first introduced by Gordon Locher from the Bartol Institute in Pennsylvania in 1936[4], only 4 years after the discovery of the neutron. It is based on the (n, α) nuclear reaction that occurs when the stable isotope ^{10}B is irradiated with thermal neutrons. The two components of BNCT, pharmaceuticals labeled with ^{10}B isotopes and thermal neutrons, have very little effects on cells individually. However, when the two components are combined, i.e. when the tissue loaded with the ^{10}B-labeled compound is irradiated with thermal neutrons, a reaction occurs which is lethal to the boron-containing cell. The thermal neutron is captured by the ^{10}B atom, forming the excited state of ^{11}B. The ^{11}B atom then immediately disintegrates to give off an alpha particle and a recoiled Lithium-7 ion, two high-energy heavy charged particles that cause radiation damage in the cells in which the ^{10}B is located.

There are several factors that make ^{10}B containing compounds ideal for NCT applications. First, the ^{10}B isotope is readily available, comprising approximately 20% of naturally occurring boron. Secondly, the ^{10}B nucleus has a very high capture cross section for thermal neutrons (3837 barns), so it is easy to achieve a reasonable reaction rate with a relatively low concentration of ^{10}B. Thirdly, the two fission products that result from the absorption of thermal neutrons by ^{10}B deposit their energy within ~ 10 μm of the reaction origin. Therefore, if the ^{10}B containing compounds can be selectively concentrated in tumor cells, these cells will receive a higher radiation dose than their normal tissue counterparts. Figure 1.1 illustrates the ^{10}B (n, α)^{7}Li nuclear reactions[5].

$$^{10}B + n_{th} \rightarrow {}^{4}_{2}He + {}^{7}_{3}Li + 2.79MeV(6\%)$$

$$^{10}B + n_{th} \rightarrow {}^{4}_{2}He + {}^{7}_{3}Li + 0.478MeV + 2.31MeV(94\%)$$

Figure 1.1. Nuclear reactions of ^{10}B and thermal neutrons

Much of the selectivity of the radiation damage provided by BNCT depends on the ability of the ^{10}B containing compounds to both selectively concentrate in tumor cells relative to surrounding normal tissues, and to have a sufficiently high absolute concentration of ^{10}B in tumor tissues. In the initial trials of BNCT back in the 1950s, the ^{10}B-labeled chemicals used did not possess this desired capability. The low selectivity of the ^{10}B-labeled drug and the shallow penetration depth of the thermal neutron beam used at the time resulted in the failure to show any efficacy in the early BNCT clinical trials that were conducted at Brookhaven National Laboratory (BNL) and at Massachusetts General Hospital (MGH)/Massachusetts Institute of Technology (MIT)[6]. In fact, the high boron concentrations in blood during irradiation resulted in damage to the normal brain vasculatures. The clinical trials in the United States were therefore terminated. Clinical work continues in Japan beginning in 1968 and for decades, the only clinical BNCT experimentation was conducted by Dr. Hatanaka[7], and later by Dr. Nakagawa[8]. With the development of ^{10}B labeled compounds with more selective tumor uptake, such as sulfhydryl-containing polyhedral borane (BSH) and boronophenylalanine (BPA), and the design of more penetrating epithermal neutron beams, clinical trials are once again being conducted in the United States, both at MIT (the Harvard-MIT BNCT Program)[9] and at BNL[10]. In Europe, an EORTC phase I clinical trial is currently underway in Petten, The Netherlands[11]. There are other European groups in Finland[12], Sweden and the Czech Republic that are preparing to start BNCT clinical trials in the near future.

The ^{10}B-labeled compounds BSH and BPA currently used in clinical trials have both been evaluated in a range of normal tissues and tumor types both in human biodistribution studies and in animal models. Their tissue distribution patterns and radiobiological characteristics are summarized in the recent review by Coderre and Morris[13]. BPA-f, a L-p-boronophenylalanine-fructose complex that is more soluble than the L-p-boronophenylalanine alone[14], was chosen for use in the U.S. clinical trials

because of its superior *in vivo* tumor targeting ability and proven effectiveness in the treatment of experimental brain tumors in rats[14-17] and in mouse[18, 19]. Advances have also been achieved in neutron beam technology. The beams currently used in clinical trials are epithermal neutron beams, which have much better penetration depth into tissue as compared to the thermal beams used in the earlier clinical trials, thus making the treatment of deep-seated tumors possible. The most recent advance in neutron beam design by the Harvard-MIT BNCT Group is the high-intensity, high-quality Fission Converter Beam (FCB)[20].

The total BNCT radiation dose in tissue is composed of several dose components: the high LET fission products of the $^{10}B(n, \alpha)^{7}Li$ reaction; the 490 KeV protons released from the $^{14}N(n,p)^{14}C$ reaction produced by the nitrogen in tissue; the recoil protons produced from the $^{1}H(n,n')p$ reaction in tissue; the structural incident gamma rays (γ) inherent in the neutron beam; and the induced γ from the $^{1}H(n, \gamma)^{2}H$ reactions. The FCB, at a reactor power of 5 MW, will have epithermal flux in excess of 10^{10} n/cm^2·s with negligible photon and fast neutron contamination, i.e., $<2 \times 10^{-11}$ cGy·cm^2/n[20]. With the lower contamination and the higher epithermal neutron, a greater proportion of BNCT dose will come from the $^{10}B(n, \alpha)^{7}Li$ reaction dose component, while reducing the treatment time to a few minutes. A thorough understanding and characterization of the pharmacokinetics of BPA in tumor and normal tissues will make more accurate treatment planning possible, and fulfill the optimal use of the FCB neutron source. It was toward that end that this research was initiated.

1.2 Research Goals

The present focus of BNCT research is the treatment of brain tumors, primarily glioblastoma multiforme, and the goal of the Phase I clinical trial is to find the maximum tolerance dose to the normal CNS. The physical dose contributed to the CNS by ^{10}B during BNCT is a function of both the neutron fluence and the ^{10}B concentration in the parenchymal tissue and the blood. The dose contribution is calculated based on the ^{10}B concentration in blood samples taken after BPA infusion because it is not practical to measure ^{10}B concentration in CNS tissue during the irradiation. The ^{10}B concentration in

tumor tissues is obtained by multiplying the blood ^{10}B concentration by a factor obtained through animal studies and human biodistribution studies[21]. The ratios of ^{10}B concentrations currently used by the Harvard-MIT BNCT program for tumor/normal brain and for normal brain/blood are 3.5 and 1, respectively.

With the completion of the fission converter epithermal neutron beam (FCB) at MIT, which will have a higher epithermal neutron fluence (1.3×10^{10} neutronsc/cm^{2}sec), future BNCT irradiations conducted by the Harvard-MIT BNCT program could be reduced from approximately 3 hours per beam to just a few minutes[20]. As mentioned above, the new beam also will have negligible fast neutron and structural gamma components, making the ^{10}B dose component more prominent, and thus more tumor selective, in the overall dose delivered. An optimal therapeutic gain is expected when patients are irradiated during a time window which has the best tumor/normal tissue ^{10}B concentration ratio, and when the ^{10}B concentration is high in the tumor.

With the current M67 beam and long irradiation time, variations in the tumor/normal tissue ^{10}B concentration ratio throughout the entire irradiation time course would be averaged out, minimizing any dosimetric impact such changes might have. However, with the reduction in unwanted dose components in the FCB and its capability to deliver BNCT in a few minutes, it is important to determine the biodistribution and pharmacokinetics of ^{10}B in both the normal brain and tumor tissues. Not only will this knowledge lead to more accurate dosimetric calculations, it will also be possible to determine the optimal time after BPA administration to deliver the neutron irradiation, thereby maximizing the dose to tumor and minimizing the dose to the normal tissues.

In phase I clinical trials in which the treatment target is the brain, in addition to the surrounding CNS tissue, other structures in the head such as the eyes and the optic tract are also of interest when studying toxicity. The biochemical rationale for the preferential uptake of BPA in tumor is thought to be an elevated rate of amino acid transport at the tumor cell membrane[22, 23]. It has been noted in the literature that there are differences in phenylalanine influx in different brain structures[24], with globus pallidus (basal ganglion) being the lowest and inferior colliculus (center for auditory reflex) being the highest. Although BPA is structurally closer to tyrosine, another large neutral amino acid, BPA is a derivative of phenylalanine. Therefore, it is conceivable

that BPA influx, and BPA concentration, might also differ in different brain structures. Knowledge of the spatial biodistribution of BPA-f in the normal brain tissues and structures such as the optic nerve is essential to be able to prescribe accurate radiation dose to radiation sensitive areas such as the optic chiasm.

This thesis research was initiated in order to gain more detailed knowledge of the temporal and spatial pharmacokinetics of ^{10}B in normal brain tissues and tumors following intravenous BPA-f administration. In the Phase I clinical trial conducted by the Harvard-MIT BNCT program, two tumor types, glioblastoma multiforme and intracranial metastatic melanoma, are currently under study. To gain insight into the pharmacokinetics of these two types of tumors, two comparable murine tumor models, GL261 glioma tumor and B16 melanoma tumor, were utilized in this research to study the time-dependent biodistribution of BPA-f.

The success of boron neutron capture therapy depends on its applicability to tumor types that cannot be treated successfully by conventional radiation therapy. It is possible that other types of tumors are better candidates for BNCT than the two currently under investigation. Attempts have been initiated to find other plausible candidates for BNCT. As part of that effort, in this thesis research an experiment was conducted to investigate whether hepatic colorectal metastasis, another tumor refractory to current treatments, could be a viable candidate, and determine whether the same favorable tumor to normal tissue ratios were seen in a different system.

It is hoped that detailed knowledge of the phamacokinetics of BPA-f could be used in future work to develop a mathematical model to describe the complex relationship between blood, tumor and normal tissue. Future research could be carried out to manipulate BPA transport through the blood-brain barrier and study ensuing changes in pharmacokinetic parameters. This, in conjunction with the blood pharmacokinetic model developed by Kiger[25], could lead to the development of treatment plans that incorporate the most advantageous BPA-f infusion schedule and time for neutron irradiation.

Chapter 2 presents the analytical tools used in this research, namely, the two techniques employed for measuring ^{10}B concentration, and the 3-compartment model used to evaluate the pharmacokinetic parameters. Chapter 3 describes the four sets of

animal experiments conducted, and discusses the results obtained and their significance and implications. The final chapter summarizes the results of this thesis, and recommends ideas for future work.

1.3 References

1. Barth, R.F., A.H. Soloway, and R.M. Brugger, *Boron neutron capture therapy of brain tumors: Past History, Current Status, and Future Potential.* Cancer Investigation, 1996. **14**(6): p. 534-550.

2. Slatkin, D.N., *A history of boron neutron capture therapy of brain tumours. Postulation of a brain radiation dose tolerance limit.* Brain, 1991. **114**(Pt 4): p. 1609-29.

3. Wazer, D., *et al.*, *Boron Neutron Capture Therapy*, in *Cancer of the Nervous System*, P.B.a.J. Loeffler, Editor. 1997, Blackwell Science: Cambridge.

4. Locher, G.L., *Biological effects and therapeutic possibilities of neutrons.* American Journal of Roentgenology, 1936. **36**: p. 1.

5. Knoll, G.F., *Radiation Detection and Measurement.* 1989, New York: John Wiley & Sons.

6. Slatkin, D.N., *A history of boron neutron capture therapy of brain tumors.* Brain, 1991. **114**: p. 1609-1629.

7. Hatanaka, H. and Y. Nakagawa, *Clinical results of long-surviving brain tumor patients who underwent boron neutron capture therapy [see comments].* Int J Radiat Oncol Biol Phys, 1994. **28**(5): p. 1061-6.

8. Nakagawa, Y. and H. Hatanaka. *Recent Studies of boron neutron capture therapy in patients with malignant brain tumors.* in *The Sixth International Symposium on Neutron Capture Therapy for Cancer.* 1995. Kobe, Japan: Plenum Press.

9. Busse, P.M., *et al. The Harvard-MIT BNCT program: overview of the clinical trials and translational research.* in *Eighth International Conference on Neutron Capture Therapy for Cancer*. 1998. LaJolla, CA: Plenum Press.

10. Coderre, J.A., *et al., Boron neutron capture therapy of glioblastoma multiforme using the p-boronophenylalanine-fructose complex and epithermal neutrons: Trial design and early clinical results.* Journal of Neuro-Oncology, 1997. **33**: p. 141-152.

11. Sauerwein, W., *et al. Status report on the european clinical trial of BNCT at Petten.* in *Eighth International Conference on Neutron Capture Therapy for Cancer*. 1998. LaJolla: Plenum Press.

12. Farkkila, M., *et al. At The Threshold of Clinical Trials-The Status of the Finnish BNCT Project.* in *Eighth International Conference on Neutron Capture Therapy for Cancer*. 1998. LaJolla, CA: Plenum Press.

13. Coderre, J.A. and G.M. Morris, *The Radiation Biology of Boron Neutron Capture Therapy.* Radiation Research, 1999. **151**: p. 1-18.

14. Coderre, J.A., *et al., Neutron Capture Therapy of the 9L Rat Gliosarcoma using the p-Boronophenylalanine-fructose Complex.* Int J Radiat Oncol Biol Phys, 1994. **30**(3): p. 643-52.

15. Coderre, J.A., *et al., Selective Delivery of Boron by the Melanin Precursor Analogue p-Boronophenylalanine to Tumors Other Than Melanoma.* Cancer Research, 1990. **50**(138-141).

16. Coderre, J.A., *et al., Control of intracerebral gliosarcomas in rats by boron neutron capture therapy with p-boronophenylalanine.* Radiat Res, 1992. **129**(3): p. 290-6.

17. Coderre, J., *et al., Selective Ablation of Rat Brain Tumors by Boron Neutron Capture Therapy.* International Journal Radiation Oncology Biology PhysicsI, 1994. **28**(5): p. 1067-77.

18. Solares, G., *et al., Biodistribution and Pharmacokinetics of p-Borono-phenylalanine in C57BL/6 Mice with GL261 Intracerebral Tumors, and Survival Following Neutron Capture Therapy*, in Progress in Neutron Capture Therapy for Cancer, D.E.M.B.J.A.B.V. Harrington, Editor. 1992, Plenum Press: New York and London. p. 475-478.

19. Saris, S.C., *et al., Boron Neutron Capture Therapy for Murine Malignant Gliomas.* Cancer Res., 1992. **52**: p. 4672-4677.

20. Kiger III, W.S., S. Sakamoto, and O.K. Harling, *Neutronic Design of A Fission Converter-Based Epithermal Neutron Beam for Neutron Capture Therapy.* Nuclear Science and Engineering, 1999. **131**: p. 1-22.

21. Coderre, J.A., *et al., Biodistribution of Boronophenylalanine in Patients with Glioblastoma Multiforme: Boron Concentration Correlates with Tumor Cellularity.* Radiation Research, 1998. **149**: p. 163-170.

22. Kabalka, G.W., *et al., Evaluation of fluorine-18-BPA-fructose for boron neutron capture treatment planning.* Journal of Nuclear Medicine, 1997. **38**: p. 1762-1767.

23. Imahori, Y., *et al., Fluorine-18-labeled fluoroboronophenylalanine PET in patients with glioma.* Journal of Nuclear Medicine, 1998. **39**: p. 325-333.

24. Hawkins, R.A., A.M. Mans, and J.F. Biebuyck, *Amino Acid Supply to Individual Cerebral Structures in Awake and Anesthetized Rats.* American Journal of Physiology, 1982. **242**: p. E1-E11.

25. Kiger III, W.S., et al. A Pharmacokinetic Model for the Concentration of Boron-10 in Blood following BPA-f Administration in Humans. in Eighth International Conference on Neutron Capture Therapy for Cancer. 1998. LaJolla, CA: Plenum Press.

Chapter 2

Analytical Tools

This chapter presents the analytical tools used in this thesis. The first section describes the ^{10}B quantification methods employed to obtain the ^{10}B concentration data. The ^{10}B concentrations are measured by two methods, prompt gamma neutron activation analysis (PGNAA) and Induction Coupled Plasma-Atomic Emission Spectroscopy (ICP-AES). An intercomparison between the ^{10}B concentrations measured by the two methods is presented. The second section shows the compartment model used to study the BPA pharmacokinetics.

2.1 ^{10}Boron Quantification

2.1.1 Introduction

^{10}B quantification is vital for BNCT treatment planning and dosimetry calculations because the dose delivered is largely dependent on the ^{10}B concentration in normal tissue and tumor. Macroscopically, ^{10}B quantification can be performed using Prompt Gamma Neutron Activation Analysis (PGNAA)[1], Inductive Coupled Plasma-Atomic Emission Spectroscopy (ICP-AES), Directly Coupled Plasma-Atomic Emission Spectroscopy (DCP-AES)[2], or Electrothermal Atomic Absorption Spectrometry[3]. Microscopically, ^{10}B quantification can be achieved using ion microscopy[4], and alpha track etching technique, such as the High Resolution Quantitative Autoradiography (HRQAR)[5, 6] developed by the Harvard-MIT BNCT group.

The exact intracellular spatial location of ^{10}B can strongly influence the biological effect of the high energy heavy particles produced following the ^{10}B (n, α) ^{7}Li reaction; therefore, microscopic quantification of ^{10}B is important for microdosimetric analysis. However, macroscopic measurements are simpler and faster than microscopic techniques. For the determination of ^{10}B concentration in blood and tissue, macroscopic measurements give sufficient data to determine the pharmacokinetics of BPA-f in various tissues as desired. This research used prompt gamma neutron activation analysis

(PGNAA) for blood ^{10}B measurements, and used Induction Coupled Plasma-Atomic Emission Spectroscopy (ICP-AES) to quantify tissue ^{10}B concentrations.

2.1.2 PGNAA Method

At the Harvard-MIT BNCT Group, boron analysis of the blood is usually performed macroscopically using Prompt Gamma Neutron Activation Analysis (PGNAA). This is the method of choice for the blood ^{10}B quantification for this thesis research. The PGNAA method is a nondestructive nuclear analytical technique that detects the 478 keV photons produced from the de-excitation of the lithium recoil nucleus resulting from the $^{10}B(n, \alpha)^{7}Li$ reaction. The number of counts integrated in the 478 keV peak is proportional to the number of boron atoms present in the sample. Figure 2.1 shows a schematic of the decay mechanism for the excited state of ^{11}B[7].

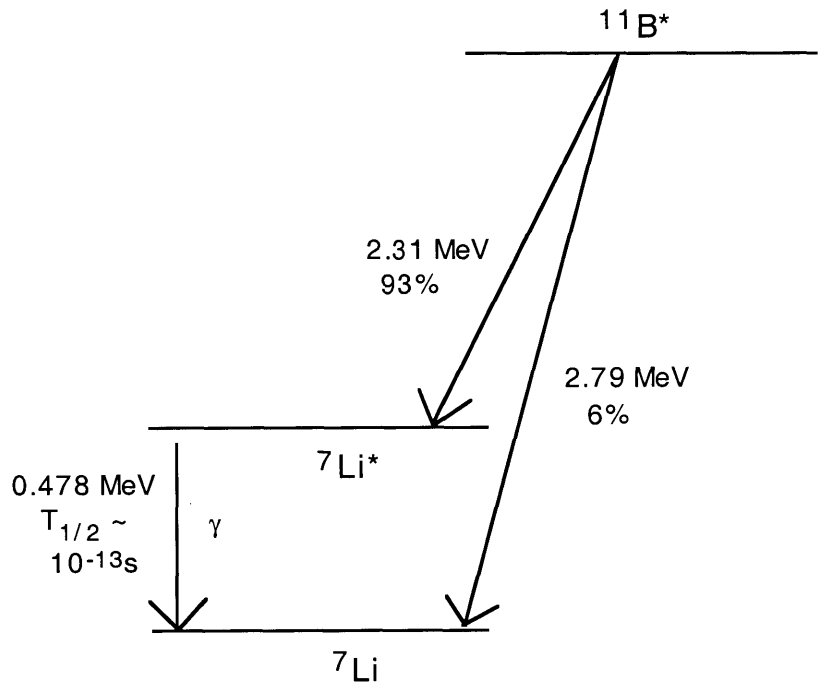

Figure 2.1 Decay Scheme of $^{11}B^*$

At the MITR-II 5 MW research reactor, the PGNAA facility is currently situated on the 4DH3 beam port and was redesigned and reconstructed by Kent Riley in 1997[8].

This led to an increase of the flux at the sample position by a factor of three (to 1.7 x 10^7 n/cm^2), an increase in sensitivity by a factor of 2.5, and a decrease in the background seen by the High Purity Germanium (HPGE) crystal[8]. The boron sensitivity is 18.6 cps/μg at the MIT-II PGNAA system, and its limit of detection is 0.25 μg[9].

For the measurement of blood samples, the samples are pipetted into cylindrical Teflon vials that are 1.5 cm high and 1.3 cm in diameter[8], and are placed manually one by one into the 4DH3 beam port of the MITR-II Research Reactor. Teflon vials are used because they will not be activated by the neutrons. The measurements usually proceed until less than 5% error in ^{10}B counts is obtained; most of the higher concentration samples have less than 3% error. For a 0.5 ml sample with a ^{10}B concentration in the 2-4 ppm range, it typically takes 20 minutes or more to reach a 5% error in ^{10}B counts. For a 0.5 ml sample with 30 ppm ^{10}B concentration, counting the sample for 1 minute will usually yield less than 2% error. System calibration is performed on each day of measurement using natural boric acid obtained from the U.S. National Institute of Standards and Technology (NIST). The standards used for the construction of the calibration curve should have the same volume as the samples to reduce the artifacts introduced by different volume and geometry. A background hydrogen count rate and a ^{10}B background count rate (blank standard) check is also performed for each reactor startup period if the reactor has been shut down in the days prior to the measurements. The background H count rate is measured by placing an empty Teflon vial into the beam. To measure the background ^{10}B count rate, deionized water of the same volume as the sample is placed in the sample position. Deionized water is used for the blank standard because its hydrogen content is similar to that of blood and tissues, about 11%. To control for possible flux variation during measurements and inhomogeneity in the sample composition and geometry, the B/H ratio method is used to calculate the ^{10}B concentrations. The sample ^{10}B concentration is obtained by comparing the B/H ratio in the sample with the B/H ratio vs. ^{10}B concentration calibration curve.

2.1.3 ICP-AES Method

Inductive Coupled Plasma-Atomic Emission Spectroscopy (ICP-AES) is an atomic excitation technique. It is insensitive to different isotopes of the same element

and is a destructive analysis technique. The principle of ICP is as follows: 1) Argon gas flows through a torch, the end of which is surrounded by a RF coil that sets up an oscillating electromagnetic field. 2) Argon ions are generated when the torch is ignited. These charged ions are caught up by the oscillating electromagnetic field and try to follow the direction of the field. 3) This causes the ions to oscillate rapidly, striking more argon atoms in the process, which in turn become ionized, generating secondary ion pairs of argon ions and electrons. 4) The number of ions rapidly increases until a steady state is reached, and a plasma is formed. 5) A peristaltic pump ensures a steady sample flow rate and introduces the samples into a cross-flow nebulizer. 6) The nebulizer vaporizes the liquid samples, and injects sample aerosols into the argon plasma. 7) When the sample atoms are introduced into the plasma, they collide with the rapidly moving argon ions and become themselves excited. 8) The excited sample atoms and ions pass through the plasma, relax to lower energy states, and emit characteristic photons. 9) A spectrometer measures the intensity of the characteristic de-excitation photons from all isotopes of boron. The number of detected photons is proportional to the amount of boron present in the sample.

To use the ICP-AES to measure tissue ^{10}B concentration, the tissue samples must first be acid-digested. The procedures are the same as sample preparation for DCP-AES, and are summarized as follows[10]. The tissue samples are weighed; for every 50 mg of tissue, 0.15 ml of nitric acid:sulfuric acid (1:1) mixture is added; digestion is allowed to proceed for an hour in a 60°C shaking waterbath. 0.5 ml of 2.5% Triton X-100 is then added to the acid-digestate, which is then placed in the 60°C shaking waterbath for another hour to complete the digestion process. Finally, the acid-digested solution is diluted to a final volume of 1 ml by adding DI water[10]. The solutions are filtered using 0.22 μm filters and their B concentrations measured using ICP-AES. Typically 0.1 ml of sample solution could be lost during the filtration process, and would be accounted for during sample concentration calculations. Since AES techniques rely on atomic emission, the chemical environment of the sample atoms will affect the number of atoms being excited. As a result, different chemical environments between the standards and the samples would cause artifacts in the calibrations. To minimize this kind of matrix effects, standards are prepared in a similar manner using natural boric acid obtained from

the U.S. National Institute of Standards and Technology. Since the standards are prepared using boric acid and the animals are injected with BPA-f, an additional standard using a known concentration of BPA-f is also included to study the possible matrix effects. Although the effects of the acids, the Triton X-100, and BPA-f are taken into account by preparing the standards the same way as the samples, since there is still difference between tissue samples and boric acid standards, this artifact could not be avoided totally

The boron standards for the ICP-AES are also analyzed with the PGNAA system to provide system cross-calibration. System calibration is performed on each day of measurement. For measurement times longer than 2 hours, the temperature in the ICP-AES machine rises, causing the machine monochromater calibration to drift. Therefore, the monochromater is reprofiled every 2 hours, and a new system calibration is conducted. The ICP-AES machine used for this research (Spectroflame ICP-D) has a B sensitivity of about 2500 cps/μg, and thus can be used to measure low B concentration or small tissue samples[9].

The calibration curve obtained gives the solution B concentrations in μg B per ml of solution. To obtain the actual B concentration in terms of μg B per gram of tissue, the solution B concentration is multiplied by the total solution volume (before filtration). The total amount of B is then divided by the weight of the tissue, thus giving the B concentration in μg/g.

2.1.4 Error Analysis

^{10}B concentrations obtained by PGNAA and ICP-AES are measured by comparing the sample count rates to that of the standard calibration curve. Therefore, in addition to the inherent statistical uncertainties, the uncertainty in the calibration curve also needs to be taken into account. In this section, a brief summary of the error analysis[7] for these measurements is presented. The following equations show the error analysis for PGNAA measurements; the error analysis for the solution concentration obtained by ICP-AES is similar, with an additional error propagation step for the uncertainties in the tissue weights, and will not be described. The nomenclature used are as follows: Area = area under the peak of interest

NCR = Net Count Rate,

BCR = Background Count Rate

b = y axis intercept

$$\sigma^2_{Area} = 2 \times Integral - Area$$

$$NCR = \frac{Area}{\Delta t} - BCR$$

$$\sigma^2_{NCR} = \left(\frac{1}{\Delta t}\right)^2 \sigma^2_{Area} + \sigma^2_{BCR}$$

$$\sigma^2_{NCR} = \frac{1}{\Delta t^2}(2 \times Integral - Area) + \sigma^2_{BCR}$$

$$\frac{^{10}B}{H} = \frac{NCR_{^{10}B}}{NCR_H}$$

$$\sigma^2_{\frac{^{10}B}{H}} = \left(\frac{1}{NCR_H}\right)^2 \sigma^2_{NCR_{^{10}B}} + \left(\frac{NCR_{^{10}B}}{(NCR_H)^2}\right)^2 \sigma^2_{NCR_H}$$

$$Concentration = \frac{\frac{^{10}B}{H} - b}{slope}$$

$$\sigma^2_{Conc} = \left(\frac{1}{slope}\right)^2 \sigma^2_{\frac{^{10}B}{H}} + \left(\frac{1}{slope}\right)^2 \sigma^2_b + \left(\frac{\frac{^{10}B}{H} - b}{slope^2}\right)^2 \sigma^2_{slope}$$

For ICP-AES measurements, the count rates measured can be directly substituted in place of the B/H ratio. As mentioned before, the use of the B/H ratio is to avoid the error that might arise if the sample has inhomogeneity in its composition or geometry, and is not applicable to the ICP-AES measurements.

Most of the PGNAA sample measurements are measured for long periods of time until the ^{10}B peak area errors are less than 3%, and the H peak errors are less than 1%. We have chosen long measuring times such that after proper error propagation is carried out to account for the uncertainty in the calibration curve, the percent error in the ^{10}B concentrations calculated would be between 5% and 7%.

2.1.5 Intercomparisons of PGNAA and ICP-AES measurements of ^{10}B concentrations in murine lungs

Experiments were conducted to ascertain that the ^{10}B quantification methods used in this thesis produce accurate and repeatable results, and that the measurements obtained by PGNAA and ICP-AES could be used together in a study.

An experiment was designed and conducted to study the repeatability of PGNAA measurements. Table 2.1 shows the results of that experiment. Not only are PGNAA measurements quite repeatable if the liquid sample is left undisturbed, even if the sample vial is taken out of the sample holder and then replaced, the results are still quite repeatable. Therefore, it seems that PGNAA measurements are quite repeatable if the sample is in liquid form with no geometric and composition inhomogeneity.

Sample #	^{10}B concentrations (ppm)
Blood 17	12.3 ± 1.0
Without movement	11.5 ± 0.9
Without movement	12.5 ± 0.9
Without movement	12.0 ± 1.0
Without movement	11.7 ± 0.8
Without movement (Avg)	12.0 ± 1.6
Blood 17	12.1 ± 0.8
Taken out then replaced	12.4 ± 0.9
Taken out then replaced	12.4 ± 1.0
Taken out then replaced	12.5 ± 0.9
Taken out then replaced	12.3 ± 0.9
Taken out then replaced (Avg)	12.3 ± 1.5

Table 2.1 PGNAA repeatability test

Another experiment was conducted using PGNAA to measure tissue samples. One lung sample was measured 5 different times, with the sample being placed in different parts of the Telfon vial. In one position, the sample was spread out at the

bottom of the vial, while in the other positions, the sample was placed to one side of the vial, and rotated 90° for each measurement. Two pieces of 30 ppm chicken liver HRQAR standards were also included as monitor checks. The results are presented in Table 2.2.

Sample	Weight (mg)	B-10 Conc. B/H Ratio	B-10 Conc.B peak alone	% difference between B/H and B alone	% difference from known conc.
lung #11 (flat on bottom)	48.3	29.8 ± 2.6	31.4 ± 2.6	5.1 %	N/A
lung #11 (left side)		30.1 ± 2.2	28.4 ± 2.3	-6.0 %	N/A
ung #11 (front side)		27.4 ± 2.2	28.1 ± 2.4	2.5 %	N/A
ung #11 (right side)		26.5 ± 2.3	34.4 ± 3.0	23 %	N/A
lung #11 (rear side)		26.1 ± 2.1	37.2 ± 3.2	30 %	N/A
30 ppm chicken liver	48.5	28.2 ± 2.6	26.7 ± 2.2	-5.6 %	6 % (B/H) 11 % (B)
30 ppm chicken liver	44.1	34.4 ± 3.0	22.6 ± 1.9	-52 %	-15 % (B/H) 25 % (B)
lung #15 (flat on bottom)	52.4	23.2 ± 1.9	29.5 ± 2.4	21%	N/A
lung #32 (flat on bottom)	37.9	19.4 ± 1.5	18.3 ± 1.5	-6.0 %	N/A
lung #31 (flat on bottom)	47.4	19.5 ± 1.7	19.3 ± 1.6	-1.0 %	N/A

Table 2.2 PGNAA measurements of lung tissues and chicken liver standards. Background B-10 count rate for 0.05 ml of DI water was 10.55 cps.

From Table 2.2, it is clear that there is variation between the ^{10}B concentrations obtained when small tissue samples were placed in different parts of the vial. However, this difference is only around 20%, and is probably due to the spatial difference in the neutron flux and detector efficiency. Also, PGNAA measurements of the 30ppm chicken liver standard used in HRQAR experiments showed a 15% difference from the known concentration. Therefore, compared with the high repeatability observed in liquid samples, it appears that PGNAA may not be the best technique to use when measuring small tissue samples if high accuracy is required.

An intercomparison experiment between PGNAA and ICP-AES was designed and carried out. Lungs from 4 healthy mice were removed at different time points after 350 mg BPA-f/kg body weight bolus injection. The lung samples were first measured by PGNAA, and then were acid-digested and measured by ICP-AES. BPA-f samples were measured at the same time to serve as a monitoring check. Table 2.3 shows the results of this comparison experiment.

mouse #	Time after BPA Injection (min)	PGNAA (ppm)	ICP-AES (ppm)	% Difference
51	119	4.5 ± 0.4	6.1 ± 0.3	26 %
42	240	1.5 ± 0.2	2.8 ± 0.2	44 %
41	6	21.1 ± 1.7	17.8 ± 0.7	-19 %
50	28	10.9 ± 0.8	12.7 ± 0.5	14 %
BPA-f (100x)		14.4 ± 1.0	14.7 ± 0.5	1.8 %

Table 2.3 PGNAA and ICP-AES ^{10}B measurement comparisons

From Table 2.3, it is clear that for the liquid sample (BPA-f), the difference between PGNAA and ICP-AES ^{10}B measurements is very small, only 1.8%. However, for tissue samples, the difference becomes greater. The difference between PGNAA and ICP-AES ^{10}B measurements is between 14 - 26%; as seen in the experiment mentioned above, this difference is within the PGNAA measurement variations detected for small tissue samples. The only significant difference between the two measurements is sample

#42, with a difference of 44.55%. This sample was collected 240 minutes after injection, when the blood ^{10}B concentration is typically around 2 ppm. Therefore, with a low ^{10}B concentration and small tissue size, this sample might have reached the lower limit of PGNAA detection limit for the time it was measured (~30 minutes). A longer measuring time might have yielded better agreement.

From these intercomparison data and the PGNAA repeatibilty tests, a few conclusions can be drawn. If the sample is of liquid form, the PGNAA and ICP-AES measurements are within a couple percent of each other. If the samples are tissues and they are small, there seems to be a difference of 14% to 26%. However, for small tissue samples, PGNAA measurements vary depending on the location of the tissues placed in the Teflon vials, and this variation is itself around 20%. Therefore, for small tissues, it appears that ICP-AES would be a better technique to use to quantify the boron concentration. In conclusion, the two techniques give accurate boron measurements, and that the ^{10}B concentrations measured by the two techniques can be used in conjunction to study the pharmacokinetics of BPA-f.

2.2 Pharmacokinetic Modeling

2.2.1 Introduction and background

In a general sense, pharmacokinetics is the study of the kinetics of absorption, distribution, metabolism, and excretion of drugs and their pharmacological, therapeutic, or toxic effects in animals and human[11]. Each drug has its own site of action, and a characteristic profile of distribution. After a drug is introduced into a biological system, the concentration of the drug at the site of action depends on several factors that may influence drug distributions to different tissues. They are: 1) plasma protein binding; 2) specific receptor sites in tissues; 3) regional blood flow; 4) lipid solubility; 5) active transport; 6) disease; 7) effect of other drug[12]. Many drugs are bound to circulating proteins, such as albumin, globulins, lipoproteins, and acid glycoprotein[12]; only the fraction of drug that is non-protein-bound can bind to cellular receptors and be transported in and metabolized at the site of action. For most drugs, however, the extent of protein binding is not large, and this fact therefore has little effect on drug distribution.

If the site of action is a well-perfused organ, such as the heart, kidneys, or liver, they usually will accumulate a higher concentration of the drug than that fat or bone, which are poorly perfused. Since cell membranes are formed by lipoproteins, if the drug is non-polar, and therefore relatively lipid-soluble, it will distribute more readily to tissue than a polar drug. A drug will accumulate preferentially in its site of action if there are specific receptors or carriers to actively transport the drug into the cells. Lastly, diseases can affect the distribution characteristics of a drug. For example, renal failure will increase the plasma concentration of a drug.

The important kinetic processes which affect the concentration of drug at the site of action are those that govern the entry of the drug into the blood, its distribution in body tissues, and its elimination from the blood by metabolism and excretion. These processes are generally "zero-order" or "first-order". Zero-order kinetics describes a drug is which the metabolism rate is independent of the amount of drug administered. When the concentration of a drug approaches a value at which its metabolizing enzymes are saturated, its rate of metabolism becomes predominantly zero-order. Most kinetic processes affecting drug disposition are first-order[12]. A first-order process is one whose rate is directly proportional to the amount of drug undergoing the process. A good example is drug plasma concentration versus time. When a bolus intravenous injection is administered, the plasma concentration at first falls rapidly, but decreases more slowly later. The rate of decrease at any time is proportional to the concentration at that time.

There are several parameters that are widely used in drug pharmacokinetics. They are 1) biological half-life; 2) apparent volume of distribution; 3) clearance[12]. For zero-order processes, the half-life is dependent on the initial concentration; the larger the initial concentration, the longer the half-life. For first-order processes, the half-life, the time required for half of the drug to disappear, is constant. The apparent volume of distribution of a drug, V_d, may be hypothetically defined as the volume of body water required to contain the amount of drug in the body if it were uniformly present in the same concentration as in the blood. It is written as

$$D_t = V_d P_t$$

where D_t is the total amount of drug in the body, and P_t is the concentration of drug in the plasma. Clearance, C, is an expression of the loss of drug from the body. It is related to the half-life and the apparent volume of distribution by the following equation,

$$C = \beta V_d = \frac{0.693 V_d}{t_{1/2}}$$

The kidney is the primary route for the excretion of drugs, therefore, it is important to determine the renal clearance, C_R. This is defined as the volume of plasma (in ml) that is cleared of a substance by the kidneys in 1 minute[12].

These parameters are useful indicators of drug pharmacokinetics. However, due to the fact that the concentration of the drug at the site of action is often unknown, to determine an accurate dosage regimen, it is important to employ compartment modeling to predict the concentration at the site of action.

2.2.2 History of Compartment Modeling in Biological Systems

The origin of compartmental analysis can be traced back to tracer studies done in the early 1920s. In order for a tracer studies to accomplish it goal of studying the dynamic behavior of a certain substance, the biological system should not be able to distinguish between the natural substance and its tracer. Tracers are usually added in small amounts so they will not disturb the steady state existing in the system as a whole. The first tracer study was done using radioactive isotopes as tracers, Hevesey used radioactive lead to demonstrate the uptake and loss of lead by the roots of *Vicia faba*[13]. As other isotopes became available, many organic compounds were synthesized to qualitatively study the metabolic processes of lipids and proteins in animal models. From these studies, it was concluded that lipids and proteins were constantly being degraded and resynthesized. Although theoretical treatments for drug kinetics have existed since 1920[13], the first adequate quantitative treatment of these tracer studies was the classical paper by Zilversmit, Entenman, and Fishler[14]. Starting in the late 1940s, the concept of compartments and the use of differential equations to describe the behaviors of tracers became increasingly important as more research was conducted to study the dynamic behaviors of biological systems.

2.2.3 A two-compartment closed system analysis of tracer study

For compartment analysis, a one compartment model is the most simple to study. It represents uptake from a constant source, or elimination of drug from the body by all routes. Since the calculation is easy, it won't be discussed here. The transport of drug can either be passive diffusion or active transport. Passive diffusion can be represented by a closed two-compartment model[11]. In pharmacokinetics, it is the amount of drug transferred across a membrane and the rate of transfer that are of interest. The rate constants can be determined from the amount of drug in each compartment. Figure 2.2 shows a system consisting of 2 compartments separated by a permeable membrane. An example of such a system is the exchange of tritium-labeled water between plasma and ascitic fluid[11]. The radioactive tracer initially introduced into compartment A is represented as R. The amount of the unlabeled substance in compartment A is denoted as Q_A, and the amount of unlabeled substance in compartment B is Q_B. The amount of the tracer in compartment A is represented by q_A, its specific activity a_A(counts/min/mg); and the amount of tracer in compartment B is q_B, and its specific activity is a_B(counts/min/mg). The first-order forward rate constant is $k_1(min^{-1})$, and the first-order reverse rate constant is $k_2(min^{-1})$. The equations describing the transport process are shown below.

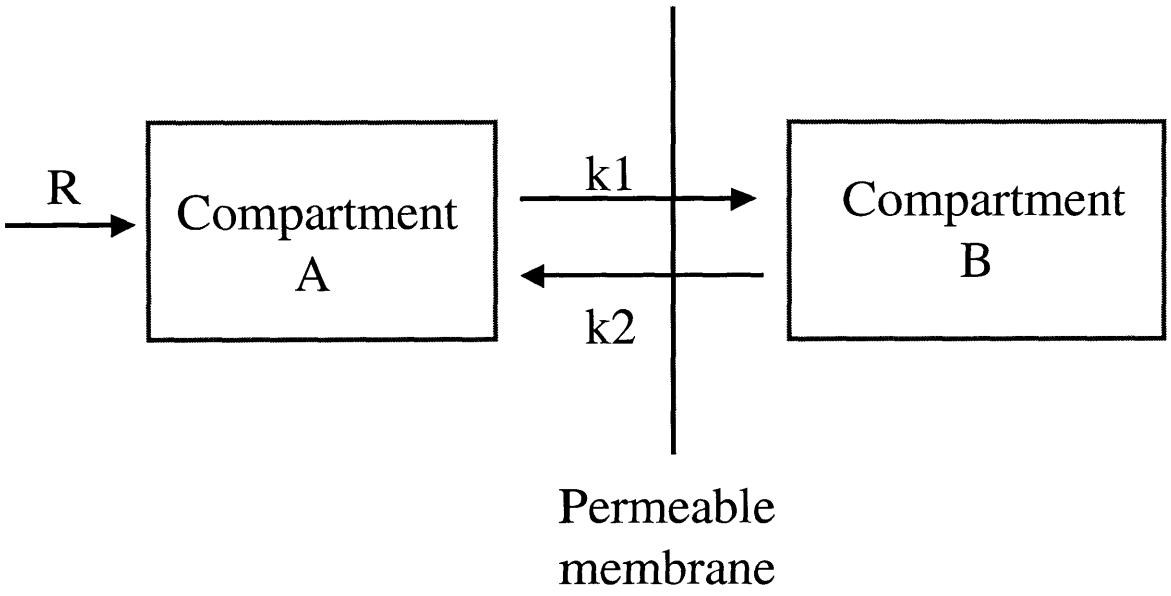

Figure 2.2 2-compartment model

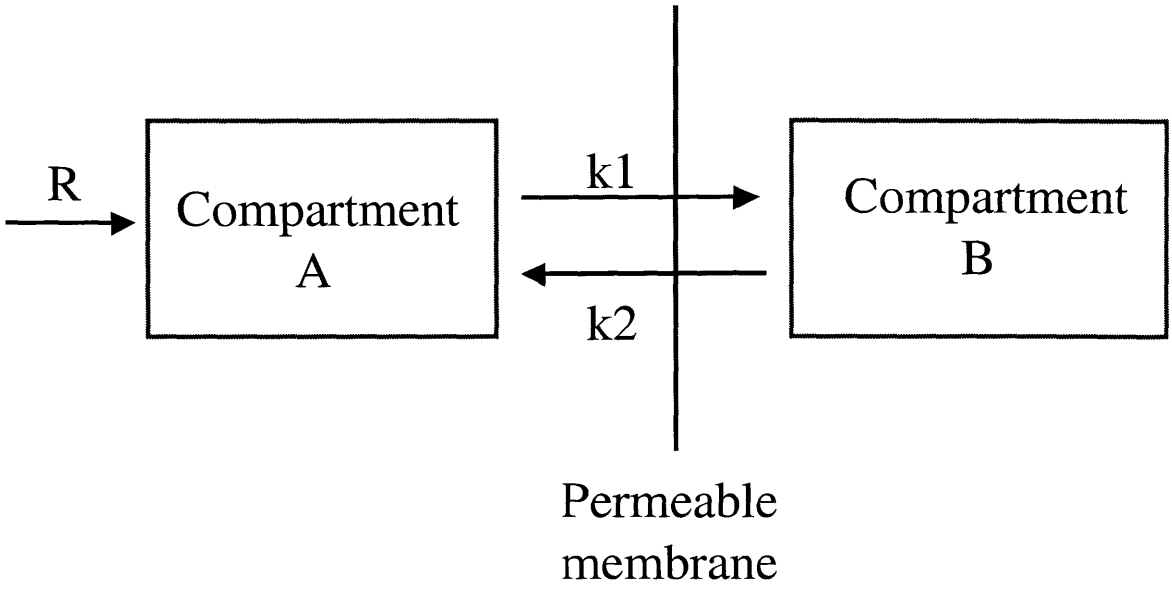

Figure 2.2 2-compartment model

The differential equations for the unlabeled substanc in steady state are

$$\frac{-dQ_A}{dt} = k_1 Q_A - k_2 Q_B = 0$$

$$\frac{dQ_B}{dt} = k_1 Q_A - k_2 Q_B = 0$$

The equations for the tracer are

$$\frac{-dq_A}{dt} = k_1 q_A - k_2 q_B$$

$$\frac{dq_B}{dt} = k_1 q_A - k_2 q_B$$

Since the specific activity of a tracer equals the product of the counting efficiency (E) and the abundance ratio, and the abundance ratio is the ratio of the amount of tracer in the compartment and the amount of the unlabeled substance in the compartment[13], the specific activity is

$$a = E\frac{q}{Q}$$

For all determinations of specific activity within an experiment, E is a constant, and could be divided out. Therefore, the rate of change of the amount of tracer is

$$\frac{dq}{dt} = \frac{da}{dt} Q$$

Substituting this into equations above,

$$\frac{da_A}{dt} = k_2 a_B \frac{Q_B}{Q_A} - k_1 a_A$$

$$\frac{da_B}{dt} = k_1 a_A \frac{Q_A}{Q_B} - k_2 a_B$$

By using the method of differential operators, the equations can be transformed into algebraic equations.

$$Dy = \frac{dy}{dt} = y'(t)$$

$$Da_A = k_2 a_B \frac{Q_B}{Q_A} - k_1 a_A$$

$$Da_B = k_1 a_A \frac{Q_A}{Q_B} - k_2 a_B$$

By rearranging the variables, these two equations become

$$a_A(D + k_1) - a_B k_2 \frac{Q_A}{Q_B} = 0$$

$$a_A k_1 \frac{Q_A}{Q_B} - a_B(D + k_2) = 0$$

These two equations can be manipulated algebraically,

$$a_B\left[D + (k_2 + k_1)\right]D = 0$$

$$a_A\left[D + (k_2 + k_1)\right]D = 0$$

and the solutions are

$$a_A = m_1 + m_2 e^{-(k_2 + k_1)t}$$

$$a_B = m_3 + m_4 e^{-(k_2 + k_1)t}$$

Since the tracer was introduced into compartment A as R at time 0, the initial specific activity for compartment A is $a_A = a_A(0)$, and $a_B = 0$. From these initial conditions, the m's are

$$m_2 = \frac{k_1 a_A(0)}{(k_2 + k_1)}$$

$$m_1 = \frac{k_2 a_A(0)}{(k_2 + k_1)}$$

$$m_3 = -\frac{k_1 a_A(0) Q_A}{(k_2 + k_1) Q_B}$$

$$m_4 = \frac{k_1 a_A(0) Q_A}{(k_2 + k_1) Q_B}$$

Therefore, the solutions to the original differential equations are

$$a_A = \frac{a_A(0)}{(k_2 + k_1)}\left[k_2 + k_1 e^{-(k_2 + k_1)t}\right]$$

$$a_B = \frac{k_1 a_A(0) Q_A}{(k_2 + k_1) Q_B}\left[1 - e^{-(k_2 + k_1)t}\right]$$

It is then possible to obtain the values of the parameters using minimization of the sum of squares.

2.2.4 Three-Compartment Modeling

In most compartmental analyses, the compartments are assumed to be homogeneous. If there is a non-homogeneous compartment, it is commonly represented by 2 homogeneous subcompartments. One of the subcompartments can exchange rapidly with the rest of the system, while the second subcompartment exchanges slowly with the first[13]. The system is then represented by a 3-compartment model. This type of model is best applicable for the BPA-f pharmacokinetics. The extracellular and intracellular ^{10}B concentrations are different in the brain; therefore, the brain cannot be treated as a

homogeneous compartment. However, there is currently no knowledge of the exact metabolism of BPA-f after administration. Since all of the quantification techniques measure the amount of B, the important question becomes whether ^{10}B atoms stay bound to the phenylalanine molecule after BPA-f has entered the body. Assuming that the ^{10}B atoms do stay bound, Imahori investigated BPA pharmacokinetics in patients with glioma by using ^{18}F-labeled BPA in a PET study. He employed a 3-compartment model to explain the PET data[15]. Figure 2.3 shows the compartment model used for ^{18}F-BPA-f pharmacokinetics.

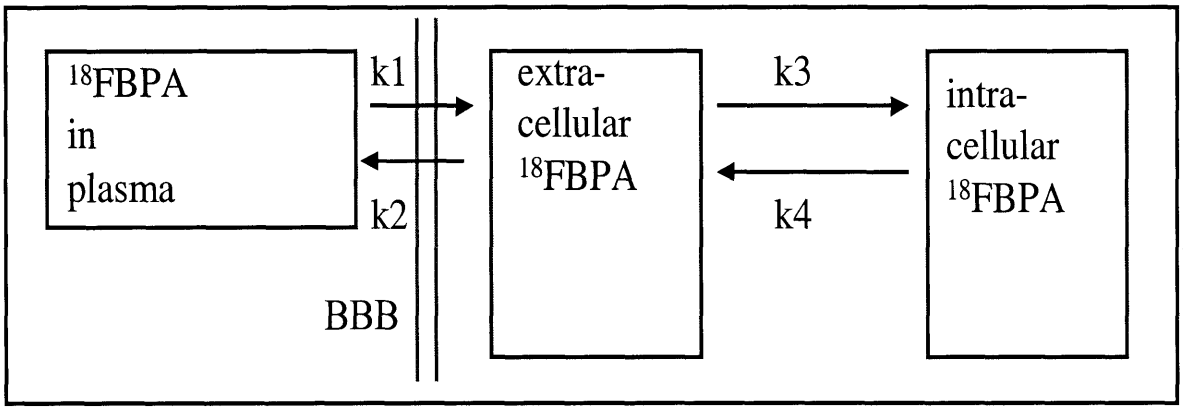

Figure 2.3 Diagram of 3-comparment model for ^{18}F-BPA-f pharmacokinetics[15]

The 3-compartment model is used in chapter 3 to determine the rate constants for GL261 and B16 intracranial tumors in mice; its kinetics are shown below. In the model shown in Fig. 2.3, the rates of change of the intracellular and extracellular ^{18}FBPA-f concentrations in tissue (C_e and C_b) are equal to the net transport of ^{18}F-BPA-f into the respective compartments.

$$\frac{d}{dt}C_e = k_1 C_p - (k_2 + k_3)C_e + k_4 C_b \qquad (1)$$

$$\frac{d}{dt}C_b = k_3 C_e - k_4 C_b \qquad (2)$$

The extracellular ^{18}FBPA-f concentration (C_e) and the intracellular ^{18}FBPA-f concentration (C_b) can be solved in terms of the BPA-f concentration in plasma (C_p) by taking the Laplace transform of equations (1) and (2),

$$SC_e(S) = k_1 C_p(S) - (k_2 + k_3) C_e(S) + k_4 C_b(S) \quad (3)$$

$$SC_b(S) = k_3 C_e(S) - k_4 C_b(S) \quad (4)$$

where initial conditions are assumed to be zero, and $C_e(S)$, $C_b(S)$, and $C_p(S)$ are the Laplace transforms of C_e, C_b, and C_p.

$$C_b(S) = \frac{k_3 C_e(S)}{(S + k_4)} \quad (5)$$

By substituting equation (5) into equation (3), and after some manipulation, $C_e(S)$ can be expressed totally in terms of $C_p(S)$ as

$$C_e(S) = \frac{k_1}{\alpha_2 - \alpha_1}\left(\frac{k_4 - \alpha_1}{S + \alpha_1} + \frac{\alpha_2 - k_4}{S + \alpha_2}\right) C_p(S) \quad (6)$$

where

$$\alpha_1 = \left(k_2 + k_3 + k_4 - \sqrt{(k_2 + k_3 + k_4)^2 - 4k_2 k_4}\right) \Big/ 2 \quad (7)$$

$$\alpha_2 = \left(k_2 + k_3 + k_4 + \sqrt{(k_2 + k_3 + k_4)^2 - 4k_2 k_4}\right) \Big/ 2 \quad (8)$$

After substituting equation (6) back to equation (5), $C_b(S)$ can then be expressed totally in terms of $C_p(S)$ as

$$C_b(S) = \frac{k_1 k_3}{\alpha_2 - \alpha_1}\left(\frac{1}{S + \alpha_1} - \frac{1}{S + \alpha_2}\right) C_p(S) \quad (9)$$

By performing inverse Laplace transforms on equations (6) and (9), we can obtain $C_e(t)$ and $C_b(t)$ in terms of the rate constants and $C_p(t)$

$$C_e(t) = \frac{k_1}{\alpha_2 - \alpha_1}\left((k_4 - \alpha_1)e^{-\alpha_1 t} + (\alpha_2 - k_4)e^{-\alpha_2 t}\right) \otimes C_p(t) \quad (10)$$

$$C_b(t) = \frac{k_1 k_3}{\alpha_2 - \alpha_1}\left(e^{-\alpha_1 t} - e^{-\alpha_2 t}\right) \otimes C_p(t) \quad (11)$$

The total amount of ^{10}B in tissues can be denoted as $C_i(t)$, and it is equal to the sum of both the extracellular and intracellular BPA-f concentrations in tissues. That is

$$C_i = C_e + C_b \tag{12}$$

Substituting equations (10) and (11) into equation (12), we obtain

$$C_i(t) = \frac{k_1}{\alpha_2 - \alpha_1}\left(\left(k_3 + k_4 - \alpha_1\right)e^{-\alpha_1 t} + \left(\alpha_2 - k_3 - k_4\right)e^{-\alpha_2 t}\right) \otimes C_p(t) \tag{13}$$

The results derived here produce the same set of equations used in the human PET studies. For the GL261 and B16 murine tumor experiments, the ^{10}B concentration in tissues (C_i) was measured by ICP-AES, and the blood ^{10}B concentration (C_p) was measured using PGNAA. The 3-compartment model was then used to determine the rate constants in GL261 and B16 murine tumors. The values of the rate constants were estimated from equation (13) by nonlinear least square regression method, and they are presented in the results section in chapter 3.

2.3 References

1. Fairchild, R.G., *et al.*, *Microanalytical techniques for boron analysis using the 10B(n,alpha)7Li reaction.* Med Phys, 1986. **13**(1): p. 50-6.

2. Barth, R.F., *et al.*, *Determination of boron concentration by means of direct current plasma-atomic emmission spectroscopy*, in *Progress In Neutron Capture Therapy*, M.D. Allen BJ, Harrington BV, Editor. 1992, Plenum Press: New York.

3. Papaspyrou, M. and L.E. Feinendegen, *Determination of Boron in Cell Suspensions Using Electrothermal Atomic Absorption Spectrometry.* Journal of Analytical Atomic Spectometry, 1994. **9**: p. 791-795.

4. Smith, D.R., *et al.*, *Ion Microscopy Imaging of 10B from p-Boronophenylalanine in a Brain Tumor Model for Boron Neutron Capture Therapy.* Cancer Res, 1996. **56**(19): p. 4302-6.

5. Solares, G.R., *et al.*, *High resolution quantitative autoradiography and its application to the microdosimetry of boron neutron capture therapy*, in *Topics in Dosimetry*, G.S. RG Zamenhof, OK Harling, Editor. 1994, Advanced Medical Publishing, Inc.: Madison, WI.

6. Kiger III, W.S., H. Pattel, and R.G. Zamenhof. *BNCT Microdosimetry of a rat glioma model with BPA-f or BSH.* in *8th Int. Symp. on Neutron Capture Therapy for cancer.* 1998. La Jolla CA: Plenum Press.

7. Knoll, G.F., *Radiation Detection and Measurement.* 1989, New York: John Wiley & Sons.

8. Riley, K.J. and O.K. Harling, *An improved prompt gamma neutron activation analysis facility using a focused diffracted neutron beam.* Nuclear Instruments and Methods in Physics Research B, 1998. **143**: p. 414-421.

9. Riley, K., *Improved Boron 10 Quantification via PGNAA and ICP-AES*, Master of Science and Nuclear Engineer Thesis, 1997, Massachusetts Institute of Technology: Cambridge, MA, U.S.A.

10. Coderre, J.A., *et al.*, *Biodistribution of Boronophenylalanine in Patients with Glioblastoma Multiforme: Boron Concentration Correlates with Tumor Cellularity.* Radiation Research, 1998. **149**: p. 163-170.

11. Notari, R.E., J.L. DeYoung, and R.C. Anderson, *Biopharmaceutics and Pharmacokinetics: An Introduction.* 2 ed. 1975, New York: marcel Dekker Inc. 285.

12. Grahame-Smith, D.G. and J.K. Aronson, *The Oxford Textbook of Clinical Pharmacology and Drug Therapy.* 1984, Oxford: Oxford University Press. 843.

13. Atkins, G.L., *Multicompartment Models for Biological Systems.* Methuen's Monographas on Biological Subjects, ed. K. Mellanby. 1969, London: Methuen & Co. LTD. 153.

14. Zilversmit, D.B., C. Entenman, and M.C. Fishler, *On the calculation of turnover time and turnover rate from experiments involving the use of labeling agents.* Journal of Gen. Physiology, 1943. **26**: p. 325.

15. Imahori, Y., *et al.*, *Fluorine-18-labeled fluoroboronophenylalanine PET in patients with glioma.* Journal of Nuclear Medicine, 1998. **39**: p. 325-333.

Chapter 3

Pharmacokinetics of BPA-f in Murine Normal Brain and Tumor Models

As stated in the introduction, with the completion of the fission converter epithermal neutron beam (FCB) at MIT, future BNCT irradiations conducted at MIT could be reduced to only a few minutes[1]. To obtain the optimal therapeutic gain, the patients should be irradiated during a time window which has the best tumor/normal tissue ^{10}B concentration ratio, and when the ^{10}B concentration is high in the tumor. Therefore, a detailed knowledge of the tumor/normal tissue ^{10}B concentration ratio as a function of time is essential. The goal of this thesis research was to determine the biodistribution and pharmacokinetics of ^{10}B in both normal tissues and in tumor tissues.

Four separate experiments are presented in this chapter. The first section describes and discusses the spatial BPA-f biodistribution in normal brain tissues for both 250 mg/kg and 350 mg/kg BPA-f administrations. The second experiment deals with the pharmacokinetics of BPA-f in intracranial GL261 murine glioma tumor model. The results are discussed and the data are fitted to a 3-compartment pharmacokinetic model. The third experiment shows the pharmacokinetics and modeling of BPA-f in intracranial B16 murine melanoma tumor model. The final experiment presents the BPA-f biodistribution in hepatic colorectal metastasis in nude mice.

3.1 BPA-f Pharmacokinetics Study in Normal Murine Brain Tissues

3.1.1 Introduction

The present focus of BNCT research is the treatment of a type of brain tumor, primarily Glioblastoma Multiforme; the Harvard-MIT BNCT Phase I protocol also includes intracranial melanoma. The normal surrounding tissue under study for the effects of BNCT radiation is the central nervous system (CNS), and the goal of the Phase I clinical trial is to find the maximum tolerance dose to the CNS. Animal studies have been conducted using the rat spinal cord model to quantify the biological effectiveness of BNCT in the normal CNS, both for BPA[2-4] and BSH[2, 5, 6]. BNCT brain tolerance

has also been studied in dogs[7-9]. From these studies, the RBEs and CBE factors of the different dose components of BNCT were determined. However, these studies did not address the issue of whether there is any spatial differential uptake of the ^{10}B compounds in various brain structures. Therefore, the brain is currently treated as a homogeneous tissue with a uniform ^{10}B concentration during treatment planning. However, the brain consists of many different structures, each with specific cognitive and motor functions; it is conceivable that there are differences in vascularity and metabolism in these structures. These variations could result in different ^{10}B pharmacokinetics in the various brain structures. In fact, some reports on amino acid transport shows that there are indeed differences in amino acid (tyrosine and phenylalanine) uptake in different brain structures[10, 11], and that the different vascularity in parts of the CNS is associated with different levels of phenylalanine influx[11]. To accurately prescribe dose and avoid harmful radiation damage to tissues that are radiation sensitive or have higher ^{10}B concentration, it is essential to determine whether there is a difference in the ^{10}B pharmacokinetics in different parts of the brain. The first series of experiments were designed to test this hypothesis, i.e., to investigate whether there is differential BPA-f uptake in different structures of the brain, such as the right and left cerebrum, the cerebellum, the brainstem and the intracranial nerves. Although not on the same scale as radio-labeled amino acid and autoradiography of the brain sections[10], this preliminary experiment may provide information that can be used to design experiments to provide better spatial resolution. The section that follows presents the methodology of the experiments and results of both the spatial and temporal biodistribution of BPA-f in the normal mouse brain.

3.1.2. Materials and Methods

Two sets of experiments were conducted. Approximately 10-week old female C57BL/6 mice were given a bolus injection of BPA-f (250 mg BPA-f/kg body weight or 350 mg BPA-f/kg body weight) through the tail vein using a 26G needle. Tail vein injection is more easily accomplished if the tail of the mouse has been warmed up. This can be accomplished by shining a heating lamp on the tail for a few minutes, causing expansion of the tiny veins on the sides of the tail. The obvious vessel observable on the

top surface of the tail is an artery, and should not be used for this purpose. The mouse is not anesthetized for tail vein injection because anesthesia will constrict the vessels.

For the 250 mg/kg group, five mice were sacrificed at each of the 6 different time points (5, 10, 15, 30, 60, and 120 min after injection); for the 350 mg/kg group, data points at 240 minutes after injection were also collected. After anesthesia (intraperitoneal Pentobarbital, 30 mg/kg body weight), the mouse is pinned spread-eagle on a wooden cutting board, and cardiac puncture is performed at the designated time points to collect blood samples. The procedures for cardiac puncture are as follows: 1) A pair of sterile tweezers with teeth is used to pick up the skin of the abdomen. The skin is cut below the diaphragm, across the width of most of the abdomen. 2) The abdominal muscle is cut slightly below the diaphragm to expose the abdominal cavity. 3) A cut is made through the diaphragm into the thoracic cavity to expose the heart. 4) The heart is penetrated at the apex with a heparinized 26G needle, and as much blood as possible is aspirated, usually no more than 0.5 ml. The blood is then deposited into a purple top specimen tube. The whole procedure, from the initiation of anesthesia to deposition of blood into tube, takes less than 5 minutes. The brain tissues were removed post mortem, and divided into right cerebrum, left cerebrum, cerebellum, brain stem and intracranial nerves. The blood was analyzed for ^{10}B concentration via the PGNAA method, while the tissues were analyzed for ^{10}B concentration by ICP-AES.

3.1.3 Results and Discussions

A total of sixty-five C57BL/6 mice were used for the normal neural tissue spatial distribution study. Thirty mice received 250 mg BPA-f/kg body weight, and thirty-five received 350 mg/kg via a bolus tail vein injection. Two separate experiments with different BPA-f doses were done to study the effect of different dose regimens on the biodistribution of BPA-f in normal brain. The BPA doses chosen correlate with the two dose regimens employed in the Harvard-MIT Phase I clinical trials. The clinical trials initially started with 250 mg BPA-f/kg body weight infused over 60 minutes. The concentration was later increased to 350 mg BPA-f/kg body weight infused over 90 minutes to increase the average ^{10}B concentration during irradiation. The 250 mg/kg cohort was sacrificed at 5, 10, 15, 30, 60, and 120 minutes after injection. The 350

mg/kg group was sacrificed at 5, 10, 15, 30, 60, 120, and 240 minutes after injection. The blood samples were analyzed for ^{10}B concentration with the PGNAA method. The ^{10}B distributions in blood as a function of time for the two concentrations of BPA-f infused are shown in figure 3.1. The mouse blood curve is remarkably similar to that of the human blood biodistribution curve[12, 13], with the characteristic bi-exponential decay. The rapid decline corresponds to redistribution of BPA-f throughout the body, while the more gradual loss of BPA-f is attributed to renal excretion.

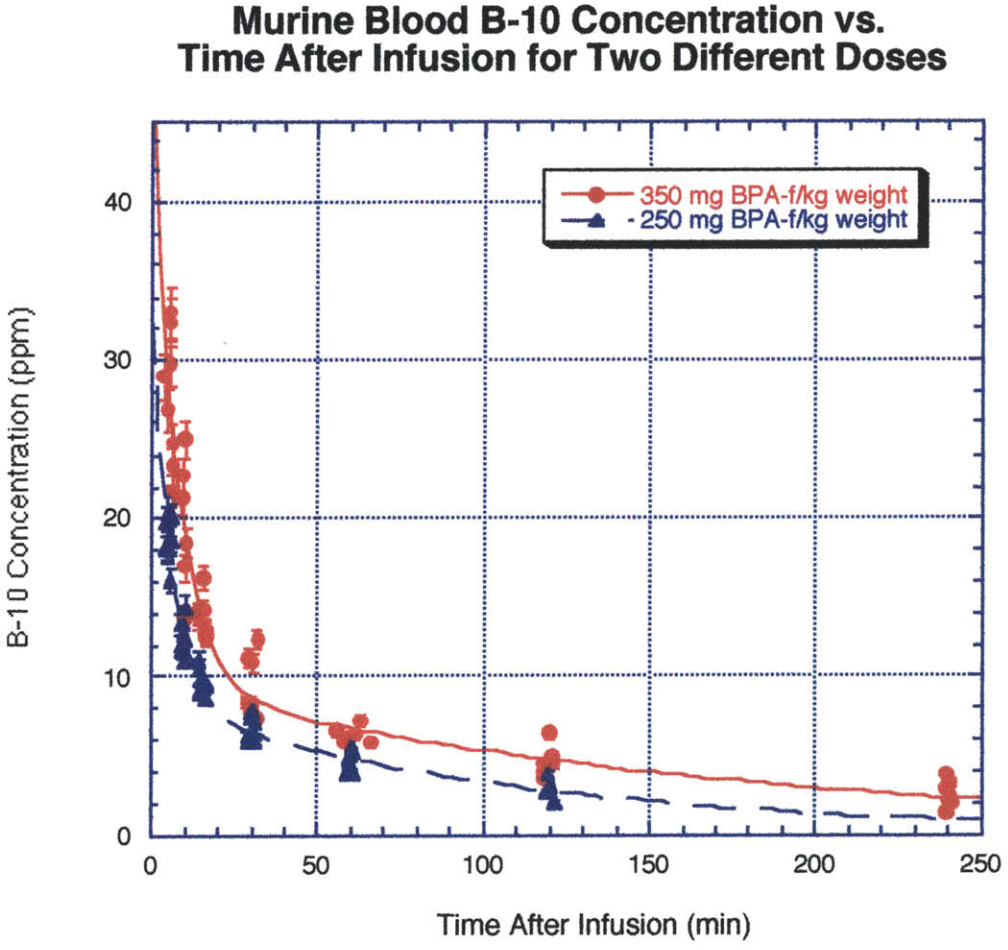

Figure 3.1 ^{10}B concentration (ppm) in blood as a function of time following a bolus tail vein injection of either 250 mg BPA-f /kg body weight or 350 mg BPA-f /kg body weight.

The neural tissues were removed at the time of sacrifice, and were separated into right cerebrum, left cerebrum, cerebellum, brain stem, and intracranial nerve. Figure 3.2 shows that in the 350 mg/kg group, the cerebellum has consistently higher ^{10}B concentration than other anatomic sites. The intracranial nerve also has a slightly higher ^{10}B concentration at all time points studied as compared to cerebrum and brain stem. The finding that there is a slightly higher ^{10}B concentration in the intracranial nerve, a radiation sensitive organ, might have important treatment planning implications. Although due to the fact that the intracranial nerve is very small, it probably will not have any significant impact on the radiation transport calculations, the dose received by the intracranial nerve will simply have its ^{10}B dose component scaled. However, if the dose to the intracranial nerve increases substantially as a result of increased ^{10}B concentration, special care will have to be taken to minimize dose to the cranial nerves, which have important sensory and motor functions in the CNS. To examine the possible effect of the higher ^{10}B concentration obtained in the intracranial nerve, a treatment plan was simulated using MacNCTPlan[14], a treatment planning software developed at the Harvard-MIT BNCT Program, and the resulted isodose contour is shown in figure 3.3[15]. In this simulation, the CT scans from one of the human subjects from the Harvard/MIT Phase I clinical trial was used. Since it is difficult to outline all the intracranial nerves, the optic tract was outline as the "tumor" region, and was assigned a ^{10}B concentration 1.3 times that of the normal brain, which is customary assigned a value of 15 ppm in the clinical trial. The Fission Coverter Beam spectrum was used as the irradiation source. From figure 3.3, it is apparent that the higher ^{10}B concentration of the optic nerve has little effect on the dose it receives. The dose received by the ipsilateral optic nerve changes from 70% to 80, and the dose received by the optic chiasm changes from 60% to approximately 67% of the prescribed maximum normal brain dose.

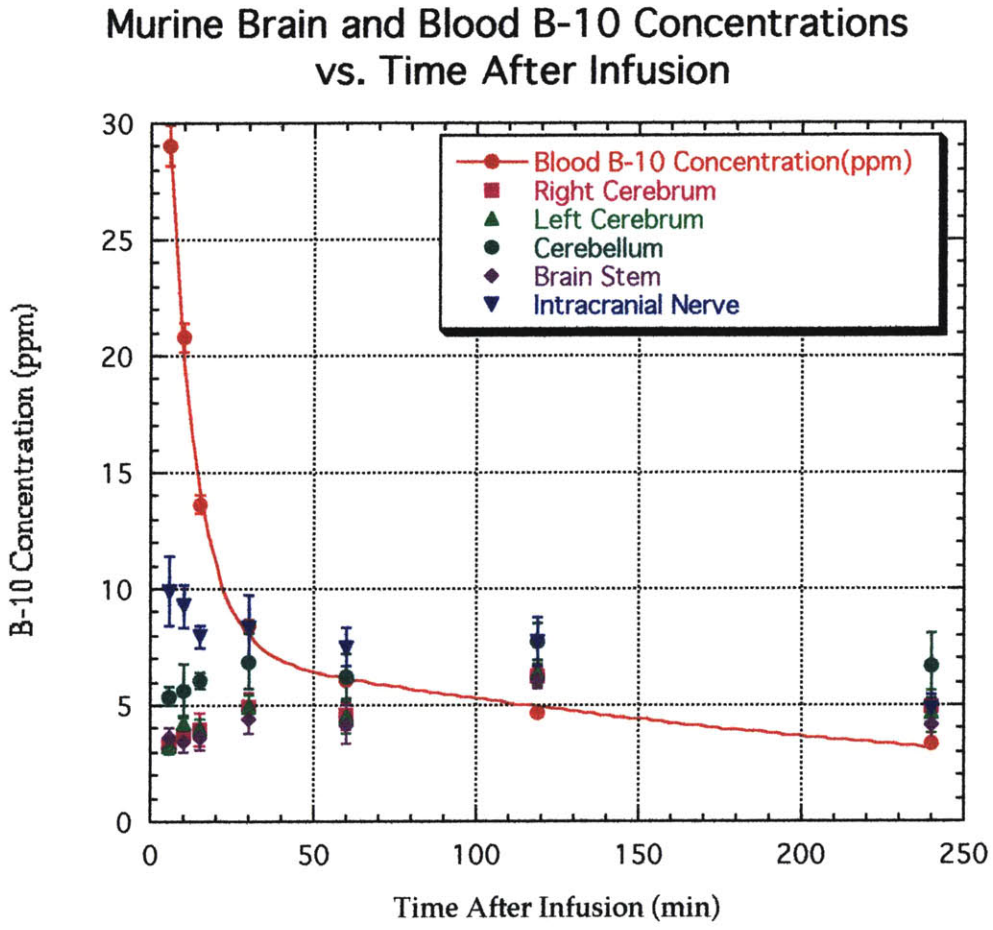

Figure 3.2 ^{10}B concentration(ppm) in blood and various murine normal neural tissues as a function of time following a bolus tail vein injection of 350mg BPA-f/kg body weight.

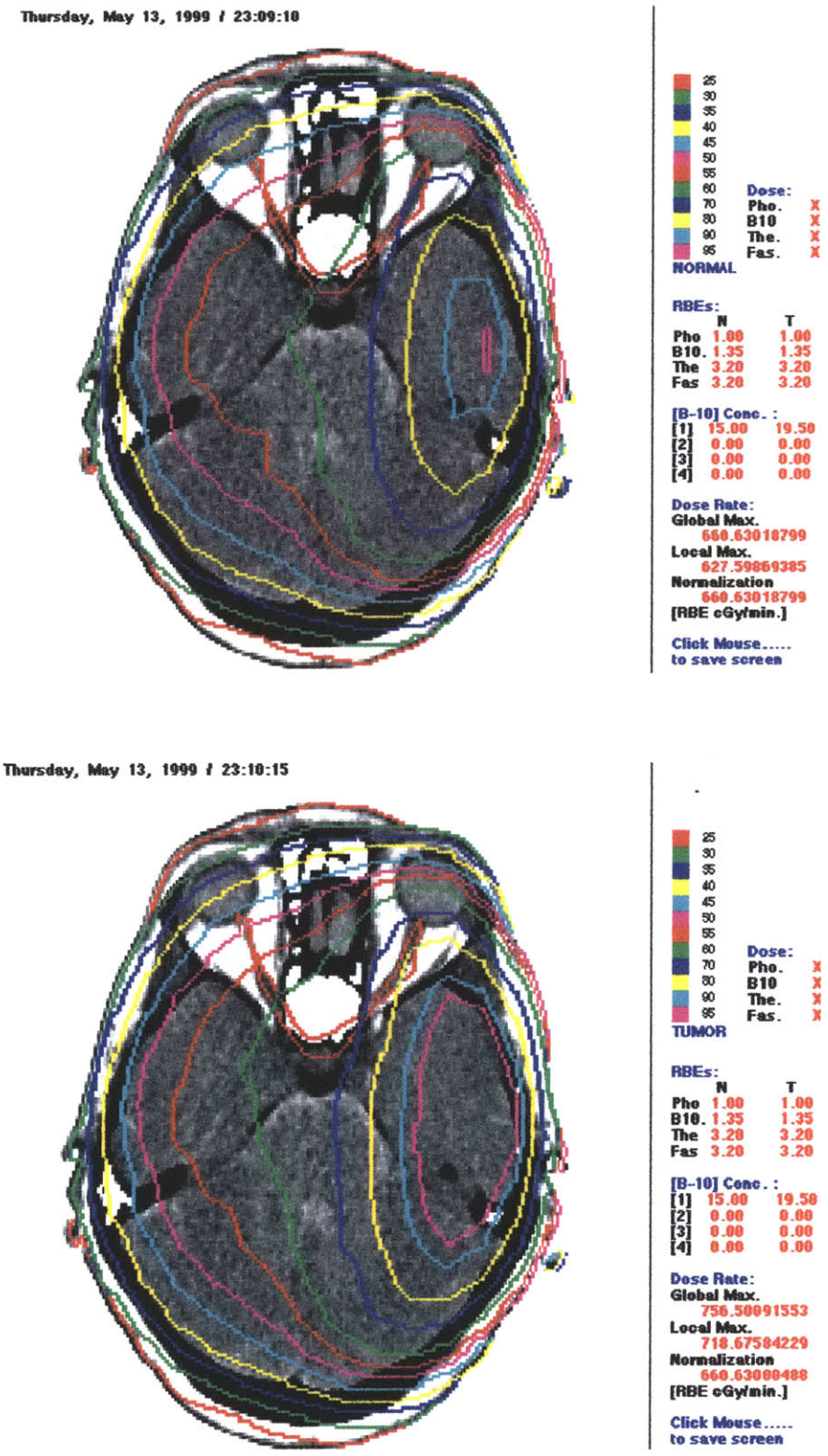

Figure 3.3 Isodose contour of optic tract and normal brain under irradiation with FCB

Figure 3.4 shows the ^{10}B distribution in blood and in normal neural tissues (averaged between right cerebrum, left cerebrum, and brainstem) as a function of time for the two concentrations of BPA-f, with the 250 mg/kg data points scaled to 350 mg/kg. They demonstrate a linear relationship between the BPA-f dose administered and the ^{10}B concentrations obtained in blood and normal neural tissues.

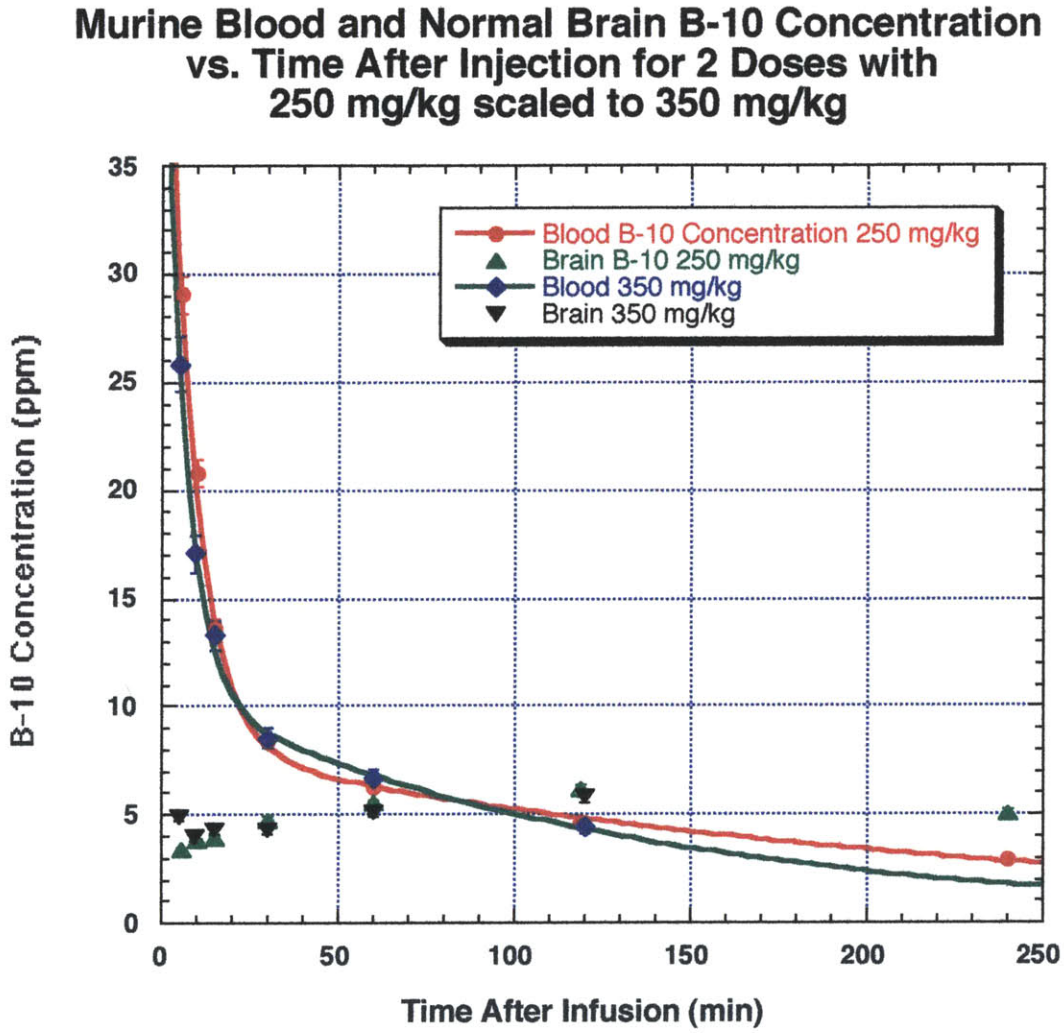

Figure 3.4 Blood and normal brain ^{10}B biodistribution (ppm) following a bolus tail vein injection of BPA-f.

As mentioned in section 2.2, researchers studying amino acid transport have long employed multi-compartment models for because they are very useful to study the pharmacokinetics of amino acids. Recently, Imahori[16] conducted cranial PET studies of human glioma subjects using ^{18}F- BPA. To explain the pharmacokinetics of the PET data, a 3-compartment model was used, which consisted of a plasma compartment, an extracellular compartment, and an intracellular compartment. From these PET data, the various rate constants were obtained for normal brain tissue and for glioblastoma multiforme. The same normal tissue rate constants were used in conjunction with blood data from mice to predict the normal brain tissue ^{10}B concentrations in mice, to determine whether mice have similar BPA-f metabolism to humans. Figure 3.5 shows the predicted normal brain ^{10}B temporal distribution and the murine experimental data points for both BPA-f doses administered.

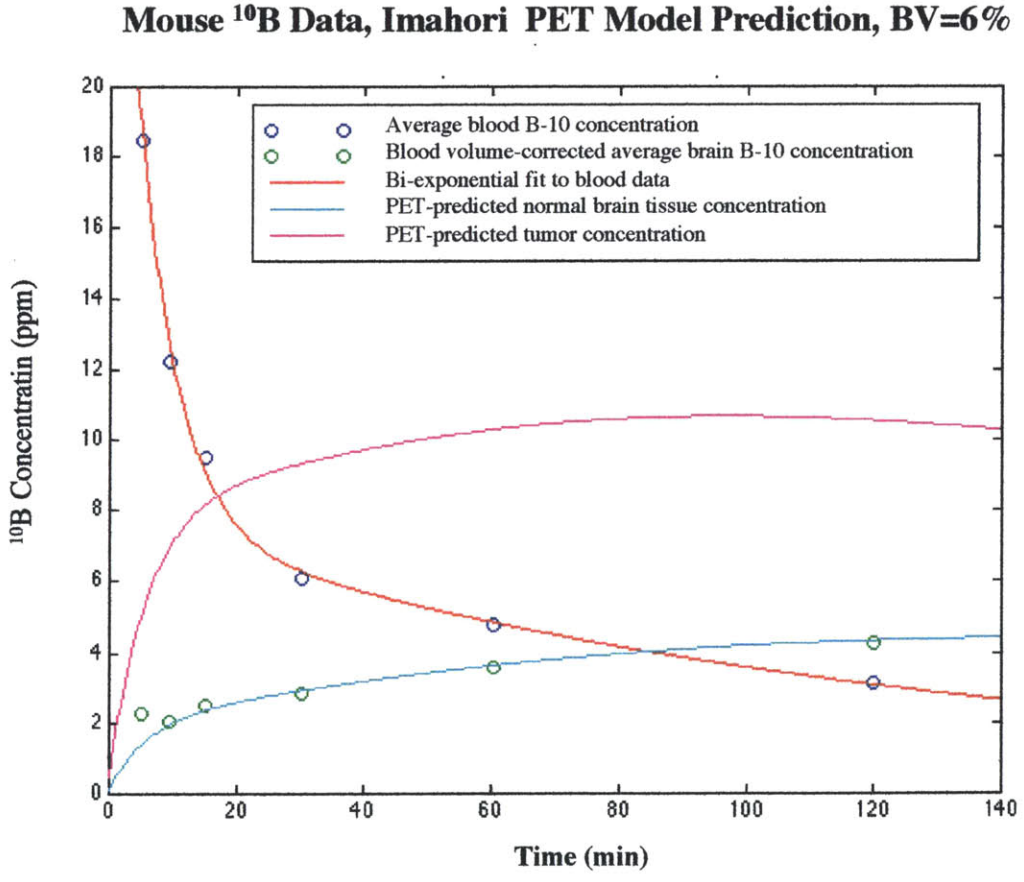

Figure 3.5 Predicted and experimental normal neural tissue ^{10}B concentrations

Figure 3.5 shows that there is excellent agreement between the experimental values for normal murine brain and the prediction using the rate constants obtained from human PET analysis. It is not clear why the earlier data points do not match as well as the later time points. However, it might be due to the fact that the PET study was conducted with a bolus injection of a trace amount of ^{18}F-labeled BPA, while in the animal study the mice received a much larger bolus injection (250 mg/kg weight to 350 mg/kg weight).

From these experimental results, several conclusions can be reached. First, the human and mouse blood ^{10}B concentration curves are similar in form; both express a characteristic bi-exponential decay, showing that the BPA-f metabolism/transport in blood is similar for both. Second, in the range of BPA-f dose currently used in the clinical trial, there is a linear relationship between the amount of BPA-f administered and the final ^{10}B concentrations reached in blood and normal brain tissues. Third, there seems to be some variation between the ^{10}B concentrations observed in the different parts of the brain; in particular, the cerebellum and the intracranial nerve ^{10}B concentrations are slightly higher than that observed in the right and left cerebrum, and the brainstem. An issue was raised regarding the time the cerebellum and the intracranial nerve were weighed. Since these tissue samples weigh less than the right and left cerebrum, and the brainstem, it is possible that with longer time interval between the time the tissues were harvested and stored in sealed eppendorf tubes and the time they were weighed, the water contents of these tissues might have changed due to drying of the samples. With the smaller samples, the drying effect would be more pronounced. Unfortunately, no experiments were conducted to study this possibility. However, since the observation that the intracranial nerve has higher ^{10}B concentrations, if confirmed, can have far-reaching implications, therefore, a treatment plan was simulated. It appears that with the FCB, the resulting dose to the optic chiasm is not significantly higher than the surrounding normal brain tissues. This small increase in the optic tract dose due to higher ^{10}B concentration may still have important clinical implication with increased radiation dose. Special care during treatment planning will have to be taken to avoid doses to the optic tract when the dose reaches 8 – 9 Gy, which is the tolerance dose of the optic tract

to single fraction radiation. In addition, although it does not appear to have significant effect, the finding that a higher ^{10}B concentration is reached in the intracranial nerve should be verified by a larger and more robust animal model. Finally, once the appropriate metabolism rate difference, namely the time scale difference between human and mouse, has been taken into account, there is not much difference observed in the normal brain metabolism of BPA-f between humans and mice. In fact, the ^{10}B concentrations predicted by the pharmacokinetic rate constants obtained from human PET studies correlate well with the ^{10}B concentrations measured in the mouse normal brain. Therefore, this murine model could be used to study the pharmacokinetics of BPA-f in normal brain tissues, and could may be a good model for studying the late radiation effects of boron neutron capture therapy in the CNS.

3.2 BPA-f Pharmacokinetics in An Intracranial Murine GL261 Glioma

3.2.1 Introduction

As mentioned previously, the selective localization of ^{10}B in the tumor is of great importance to the success of BNCT, as is the absolute amount of ^{10}B in tumor as well as the tumor-to-blood and tumor-to-normal tissue ^{10}B concentration ratios. Animal studies have demonstrated that Boronophenylalanine (BPA) is taken up preferentially by different tumors[17], including melanoma[18] and rat 9L gliosarcoma[19]. Almost all the animal studies examining BPA biodistribution and BNCT radiation effect on tumor and normal brain have used the rat 9L gliosarcoma model. However, since previous work in this laboratory by Dr. Solares[20, 21] used the murine glial tumor GL261, it was once again selected as the system to be studied. In the previous GL261 experiments in this laboratory, intracerebral tumor was induced by inoculating the mice with GL261 tumor fragments grown in the flanks of other C57BL/6 mice. In the present work, the GL261 cells used for inoculation were grown *in vitro*. Single cell suspension inoculation

has the advantage that the tumor will grow more dispersively and not be confined to the location of the tumor fragment.

3.2.2 Materials and Methods

Murine Glioma Model: Cryopreserved tumor fragments of the mouse glioma GL261 cell line were obtained from the Division of Cancer Treatment and Diagnosis Tumor Repository at the National Cancer Institute (Frederick, Maryland). This is a primary mouse brain tumor cell line that was induced in the brains of C57BL/6 mice after intracerebral implantation of methylcholanthrene pellets.

Tumor Cell Growth in Tissue Culture: The tumor fragments came in frozen vials shipped in dry ice. The vial is thawed by immersion in a 37°C waterbath for up to 1 minute; if the vial is kept in the waterbath for longer than 1 minute, the DMSO present in the freezing medium will kill the cells. The vial is quickly wiped with a paper towel saturated with 70% ethanol and brought into a laminar flow hood that has been thoroughly wiped down with 70% ethanol. Careful aseptic technique is important throughout the procedure. The contents of the vial is rapidly poured into a 15 ml conical centrifuge tube containing 10 ml of Dulbecco's Modified Eagle Medium (DMEM with 4.5 g/L Glucose; GIBCO Laboratories Life Technologies Inc., Grand Island, NY) supplemented with 10% fetal bovine serum (FBS, heat inactivated in a 60°C water bath for 30 minutes; SIGMA Chemical Company, St. Louis, MO). The cells are centrifuged for 2 minutes at 1000 RPM; the fetal bovine serum will neutralize the effect of the DMSO and help to reduce the damage to the cells. The supernatant is discarded using a sterile glass pasteur pipet, and the tumor fragments are placed in a 100 mm culture dish. The tumor is minced into small pieces with a sterile scalpel and placed in a 50 ml centrifuge tube containing 20 ml DMEM. After centrifuging the tumor pieces are allowed to settle and the supernatant is poured off. The following reagents are added; 8 ml of DMEM, 1 ml of collagenase (4500 U/ml; Sigma Chemical Company, St. Louis, MO) and 1 ml of DNAse (1 mg/ml; Sigma Chemical Company, St. Louis, MO). The cells are then incubated at 37°C for 10 minutes in a shaking waterbath and spun at 1000 RPM for 5 minutes; the supernatant is discarded. The cells are resuspended in a solution

containing DMEM, collagenase and DNAse as before, and are then incubated at 37°C for 15 minutes in a shaking waterbath. Additional 1 ml DNAse is added to the cells. The cells are then agitated for another 5 minutes at 37°C in a shaking waterbath, and filtered through a piece of sterile gauze into a 15 ml centrifuge tube to remove clumps. This whole procedure will break up the tissue fragments and release individual cells. The cells are spun for another 5 minutes at 1000 RPM and resuspended in 10 ml DMEM. After being vortexed a little, the cells are spun for 5 minutes at 1000 RPM and the supernatant is discarded. Finally, the cells are resuspended in 10 ml DMEM with FBS, and placed into 2 or 3 100 mm cell culture dishes which are incubated at 5% CO_2 and 37°C.

The culture dish is checked for cell growth every couple of days. Initially, the dish should not be moved so that the cells will have a chance to attach to the bottom of the dish and grow. The medium is chanced when it turns color from pink or red to orange. The cells are maintained in Dulbecco's Modified Eagle Medium (GIBCO Laboratories Life Technologies Inc., Grand Island, NY) supplemented with 10% fetal bovine serum (FBS; SIGMA Chemical Company, St. Louis, MO), 1% L-Glutamine (GIBCO), 100 units/ml of penicillin G (GIBCO) and 100 mg/ml streptomycin (GIBCO)(2). When the cells become confluent, cells are split using the following procedures. First, the flask is removed from the incubator and placed into the hood. The old medium is asparated out using a sterile glass pasteur pipet. For a 75 cm^2 culture flask, 2 ml of cell dissociation solution (SIGMA Chemical Company, St. Louis, MO) is added, for a 150 cm^2 culture flask, 3 ml of cell dissociation solution is added. The flask is returned back to the incubator for 3 to 5 minutes. The cell dissociation solution is gentler to the cell membranes than the trypsin usually used in cell culture work. The flask is then removed from the incubator, shaken and agitated for a short while so the cells will detach from the bottom of the flask. The sides and the bottom of the flask are rinsed by adding 8 ml of medium. By pipetting up and down a few times, the cell clumps are broken up into single cell suspension. A couple of new flasks are brought into the hood, for a 75 cm^2 culture flask, 1 ml of the cell suspension is added to 20 ml of medium, for a 150 cm^2 culture flask, 1 ml of the cell suspension is added to 30 ml of medium. The medium is gently swirled around the flask so the cells will be homogeneously mixed, the new flasks are then returned to the incubator.

Generation of Brain Tumors: For the initiation of an intracranial tumor, a 10 week old female C57BL/6 mouse (Taconic, Germantown, NY) was anesthetized (intraperitoneal Pentobarbital, 30 mg/kg body weight), and the head was shaved. Using aseptic technique, the scalp was incised, and the tumor cell suspension (4×10^4 cells in 0.02 ml of medium) injected into the mouse skull at a point 4 mm to the left of the midline and 2 mm above the bregma at a depth of 4 mm using a 30-gauge needle. This technique resulted in a locally expanding tumor in most of the mice (~ 80% take rate). If no stereotactic positioning apparatus is available, the inoculation is done as follows: the 30G needle is held vertically, and used to drill a hole into the skull and the dura at a position just posterior to the coronal suture and lateral to the midline. When the bevel of the needle is just totally immersed, approximately 4 mm deep, the cell suspension is slowly injected into the brain. Approximately 2 – 3 weeks after tumor implantation, the mice are then given a BPA-f (350 mg/kg) bolus tail vein injection.

Experimental Procedure: Approximately 12 week old female C57BL/6 mice were given a bolus injection of BPA-f (350 mg BPA-f/kg body weight) through the tail vein using a 26G needle. Figure 3.6 shows a mouse hunched over and sitting in one corner of the cage, typical signs to look for when trying to determine whether a tumor has grown inside a mouse's brain. Lack of appetite, lethargy, and an obvious hunch in the back, usually indicate that a sizable tumor; the hunched back occurs when the meninges become infected or are invaded by foreign cells.

Three or four mice were sacrificed at each of 7 different time points (5, 10, 15, 30, 60, 120 and 240 minutes after injection), with additional 1 or 2 mice sacrificed at various time points such as 40, 90, and 180 minutes. Cardiac puncture as discussed in section 3.1.2 was performed to collect blood samples. The tumor tissue and normal brain tissues were removed post mortem, and separated into right cerebrum, left cerebrum, cerebellum, brainstem, intracranial nerves and tumor. The blood ^{10}B concentration was analyzed by PGNAA method, and the tissues were analyzed for ^{10}B concentrations by ICP-AES after being acid-digested.

Figure 3.6 A picture of a mouse displaying typical signs of having an intracranial tumor. Note the hunched back.

3.2.3 Results and Discussion

For this set of experiments, 12 weeks old female C57BL/6 mice bearing intracranial glioma tumor GL261 were injected with 350 mg BPA-f/kg body weight via a single bolus through the tail vein, and were sacrificed at the various time points. The blood, normal brain tissue and tumor were removed and analyzed for ^{10}B concentration. The time dependence of ^{10}B accumulation in glioma tumor and normal brain tissue is shown in figure 3.7, and their ratios are shown in figure 3.8. It can be seen from figure 3.7 that GL261 cells quickly take up BPA-f after injection, with the ^{10}B concentration in GL261 cells up to 8-11 times that of normal brain tissue at 5 -15 minutes after BPA-f injection. Both the tumor: blood and tumor: normal brain ^{10}B concentration ratios vary with time. The ^{10}B concentration in GL261 tumor rapidly decreases for later time points, it becomes about 5 times higher than that of normal brain at around 60 minutes, and further decreases to approximately only 2 times higher than brain at 240 minutes after injection. However, the ^{10}B concentration in GL261 tumor is consistently higher than the ^{10}B concentration in normal brain tissues at all times studied. This is qualitatively

consistent with human GBM biopsy data[22], although the ratios obtained in GL261 and in human glioblastoma are different. This may due to the fact that in glioblastoma biopsies, the extent of necrosis in the tumor is not known. As shown by Coderre[22], tumor ^{10}B concentration correlates with the cellularity of the tumor samples. It may also due to the fact that tumor vascularity varies among different tumor lines. However, this result confirmed that blood, normal brain, and tumor all have quite different BPA-f pharmacokinetics. A detailed knowledge of the pharmacokinetic behaviors of these tissues could have important practical implications for treatment planning.

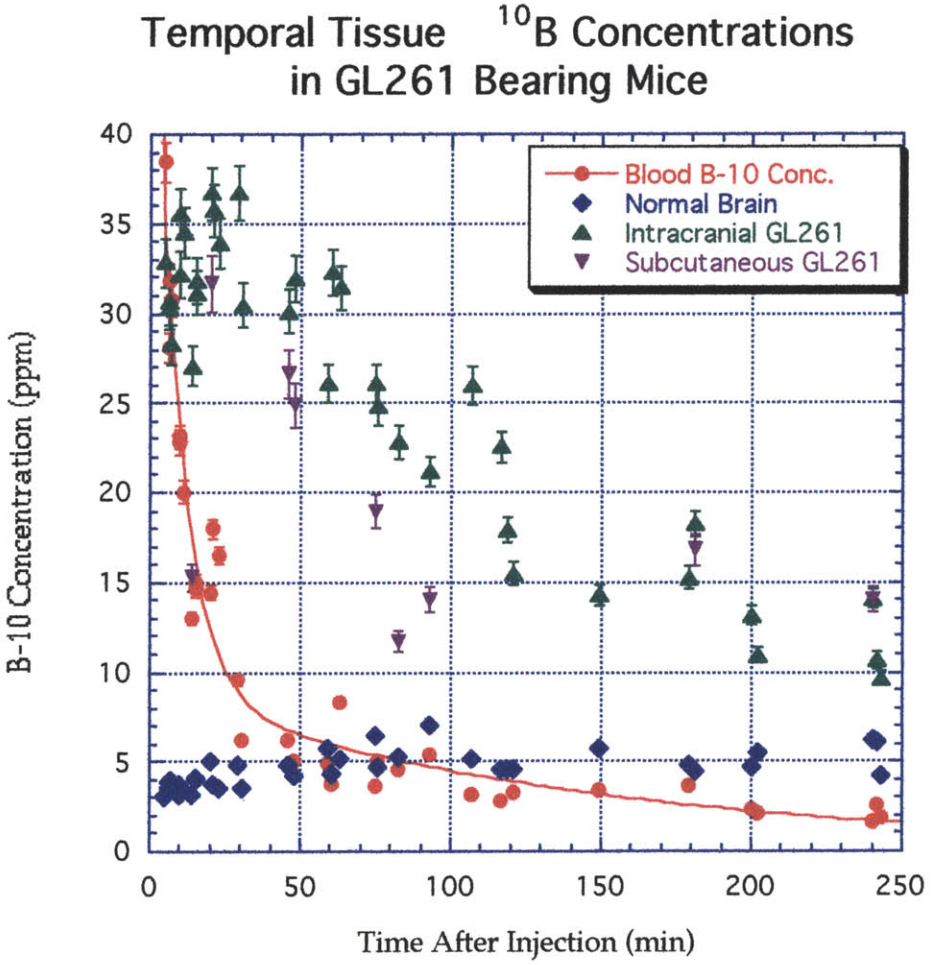

Figure 3.7. Boron concentration (ppm) in blood, brain and GL261 tumor as a function of time following a bolus tail vein injection of 350 mg BPA-f /kg body weight.

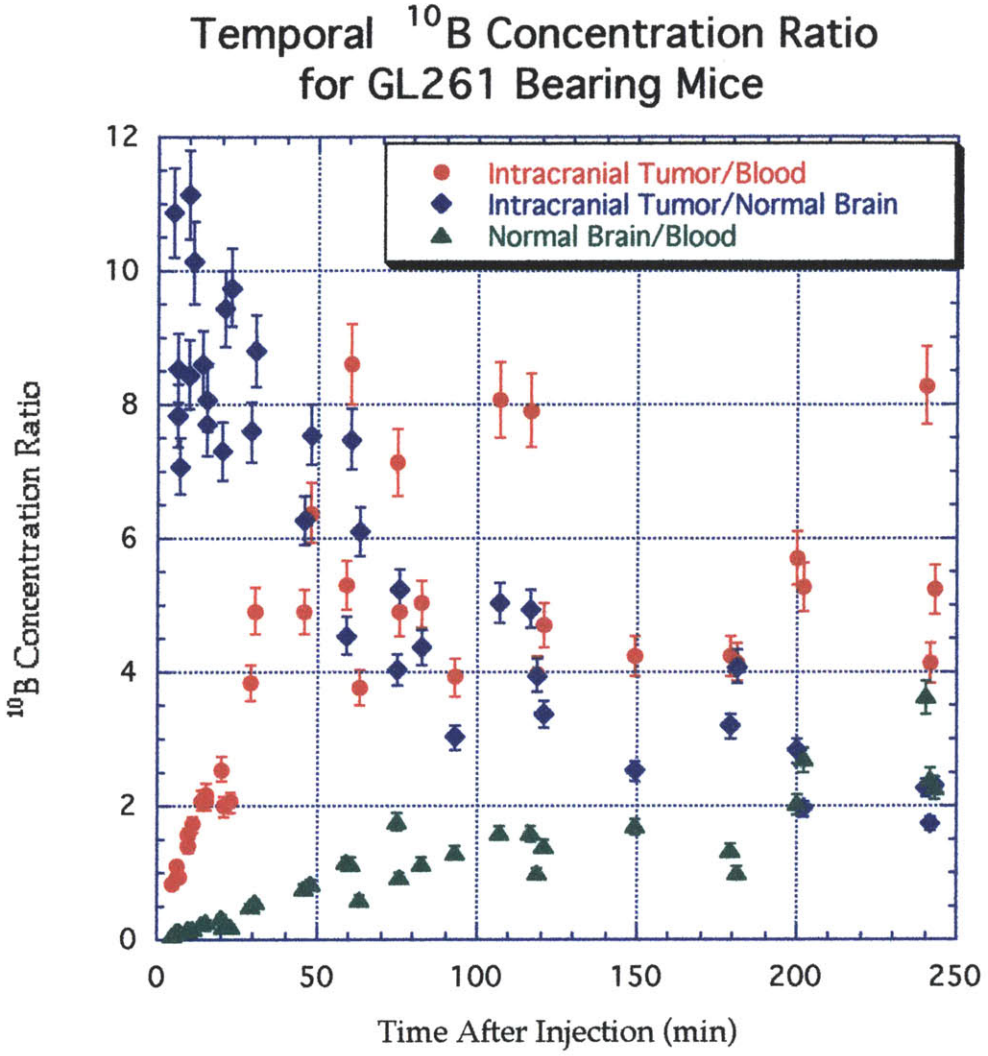

Figure 3.8 ^{10}B Concentration Ratios for Intracranial GL261/Blood, Intracranial GL261/Normal Brain, and Normal Brain/Blood.

By using the 3-compartment model detailed in section 2.3, and by minimizing the sum of the squares of the residues, the rate constants for the compartment-model of BPA-f pharmacokinetics for normal brain and GL261 tumor were obtained. The values for k1 through k4 for the normal brains are 0.01 ml/g/min, 0.25 min^{-1}, 0.033 min^{-1} and 0.011 min^{-1}, respectively, which are very close to those observed by Imahori[16] in the human PET studies (0.011 ml/g/min, 0.025 min^{-1}, 0.033 min^{-1} and 0.009 min^{-1}, respectively). The values for k1 through k4 for the GL261 tumors are 0.178 ml/g/min, 0.181 min^{-1},

0.091 min^{-1}, and 0.036 min^{-1}, respectively. These values differ substantially from the values Imahori obtained for GBM, which are 0.027 ml/g/min, 0.041 min^{-1}, 0.029 min^{-1} and 0.013 min^{-1}, respectively. There are several reasons why these values are different. The first is that different tumor lines were used; differences in BPA-f uptake metabolism can contribute to the differences in influx and efflux rates. In addition, the vascularity of the tumor lines is different. Lastly, the PET study averaged over large tumor areas including necrotic areas, while the GL261 is well vascularized; this factor likely contributed to different observed ^{10}B concentrations and the distinct pharmacokinetics. Figure 3.9 shows the experimental data and the fit of the 3-compartment model using the k's derived. Figures 3.10 and 3.11 are hemotoxlyn and eosin stained histological sections of both normal brain and GL261 tumor. They are included to demonstrate the vast differences in nuclear mass and growing pattern between normal brain and tumor.

GL261 Tumor and Normal Brain ^{10}B Data with Least Square Fit, BV6%

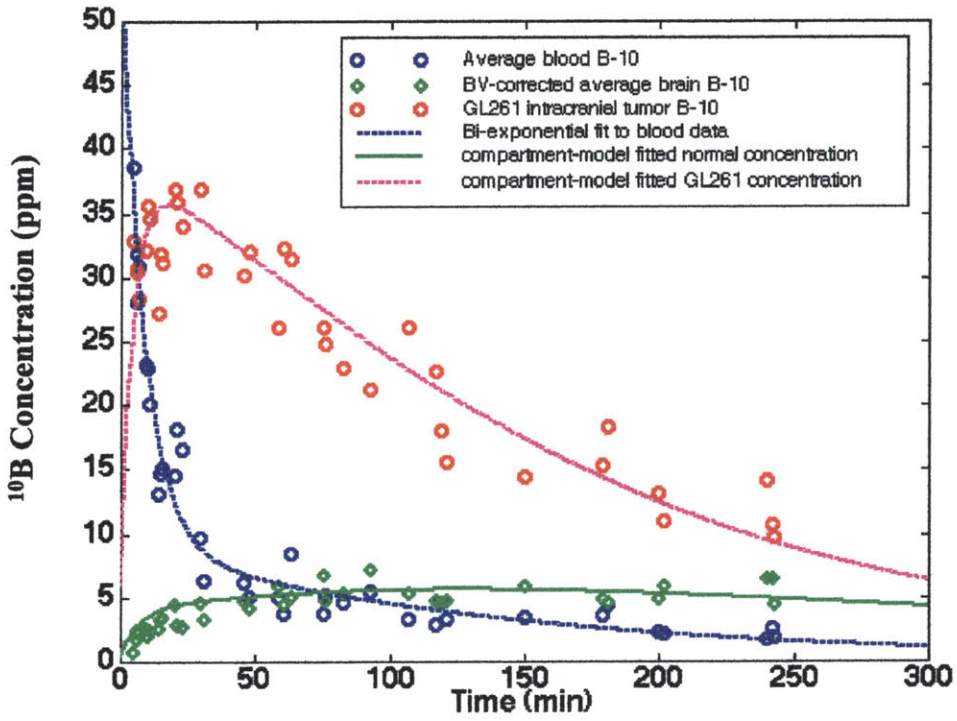

Figure 3.9 Experimental data of GL261 tumor and normal brain fitted to the three-compartment model.

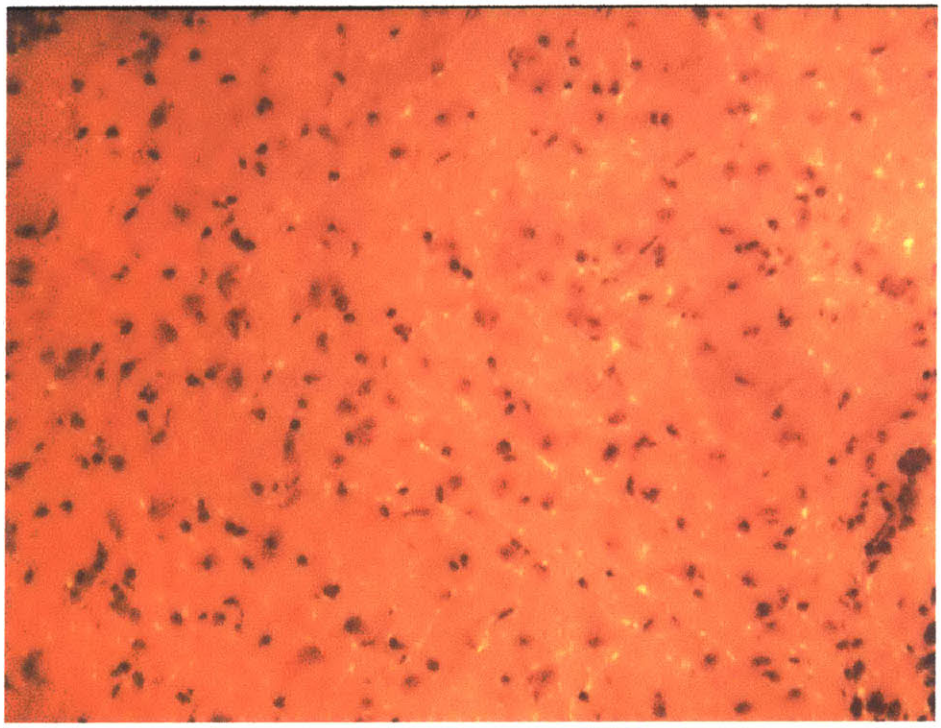

Figure 3.10 H & E stained histological section of normal murine brain.

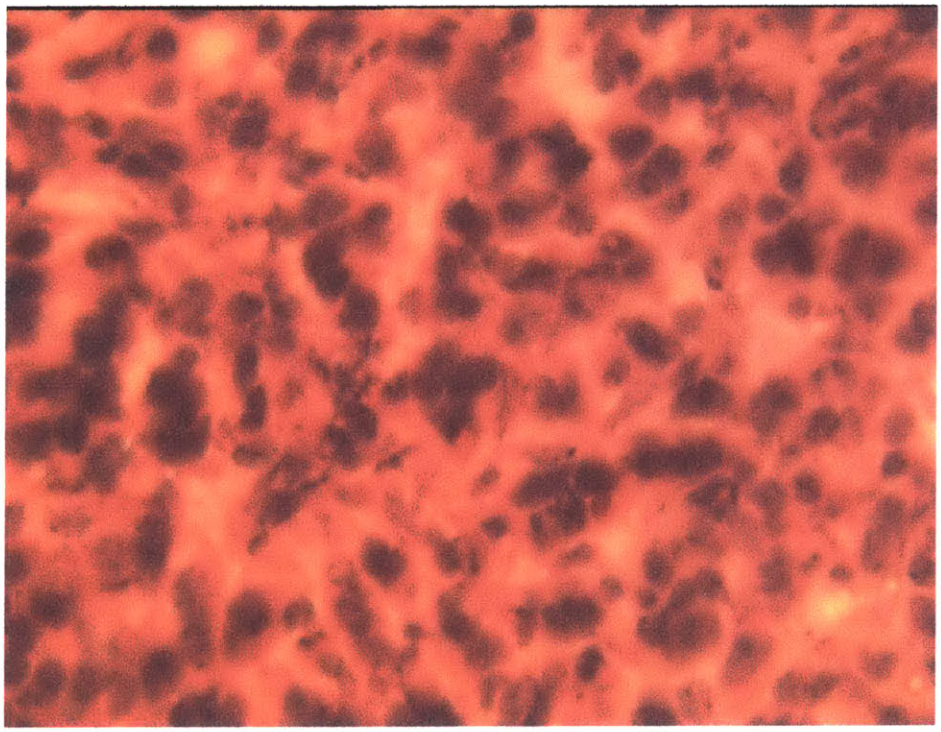

Figure 3.11 H & E stained histological section of GL261 murine glioma tumor

3.3 BPA-f Pharmacokinetics Study in B16 Melanoma bearing Murine Brains

3.3.1 Introduction

In addition to Glioblastoma Multiforme, intracranial metastatic melanoma is another tumor type currently under investigation in the Harvard-MIT Phase I clinical trial. From the results of two subjects with intracranial melanoma, BNCT appears to be promising for the treatment of such disease[23]. This observation is in line with the data collected from various human and animal models of melanoma[18, 24-26]. Melanoma is a cancer cell line that exhibits excellent uptake and accumulation of BPA. However, as in the case of glioblastoma multiforme, to be able to treat intracranial melanoma effectively without exposing the normal brain to high doses of radiation, it is important to know the full pharmacokinetics of BPA-f in intracranial melanoma tumor and its relationship to blood and normal brain BPA-f pharmacokinetics. The combined results from the BPA-f pharmacokinetics of two different intracranial tumors could provide insights into the transport and the pahrmacokinetics of BPA-f in general.

3.3.2 Materials and Methods

Murine B16 Melanoma Model: B16 murine melanoma cells were obtained from the Department of Cancer Pharmacology at Dana Farber Cancer Institute, courtesy of Dr. Emil Frei's laboratory. The tumors were removed aseptically from the flanks of C57BL/6 mice (Taconic, Germantown, NY). Using the same method detailed in section 3.2.2 for harvesting single tumor cells from tumor fragments, a B16 tumor cell suspension was obtained. Tumor cells were then grown and maintained in Dulbecco's Modified Eagle Medium (DMEM with 4.5 g/L Glucose; GIBCO Laboratories Life Technologies Inc., Grand Island, NY) supplemented with 10% fetal bovine serum (FBS; SIGMA Chemical Company, St. Louis, MO), 1% L-Glutamine (GIBCO), 100 units/ml of penicillin G (GIBCO) and 100 mg/ml streptomycin (GIBCO).

Generation of Brain Tumor and Subcutaneous Tumor: For the initiation of intracranial tumor, a 10 week old female C57BL/6 mouse (Taconic, Germantown, NY)

was anesthetized (intraperitoneal Pentobarbital, 30 mg/kg body weight), and its head was shaved. Using aseptic technique, the scalp was incised, and the tumor cell suspension (4 x 10^4 cells in 0.02 ml of medium) was injected into the mouse skull at a point 4 mm to the left of the midline and 2 mm above the bregma at a depth of 4 mm using a 30-gauge needle. This technique resulted in an invasively expanding tumor in all of the mice. Half a million cells were also injected into the subcutaneous area above the right hind leg of the mice. Approximately 10 – 16 days after tumor implantation, the mice were then given a BPA-f (350 mg/kg) bolus tail vein injection.

Experimental Procedure: Approximately 12 week old female C57BL/6 mice were given a bolus injection of BPA-f (350 mg BPA-f/kg body weight) through the tail vein using a 26G needle. Five mice were sacrificed at each of 7 different time points (5, 10, 15, 30, 60, 120 and 240 minutes after injection). Cardiac puncture was performed to collect blood samples. The tumor tissue and normal brain tissues were removed post mortem, and separated into right cerebrum, left cerebrum, cerebellum, brain stem and intracranial nerves. For animals with sizable subcutaneous melanoma lesions, the subcutaneous melanoma and skin were also removed for analysis. The blood was analyzed by PGNAA and the tissues were first acid-digested and then analyzed by ICP-AES.

3.3.3 Results and Discussion

For this set of experiments, 12 week old female C57BL/6 mice bearing intracranial melanoma tumor B16 were injected with 350 mg BPA-f/kg body weight via a single bolus through the tail vein, and were sacrificed at the various time points. The blood, normal brain tissue and B16 tumor were removed and analyzed for ^{10}B concentrations. Some of the animals also had sizable subcutaneous melanoma tumor nodules (50 mg< tumor weight< 100 mg) in their right flanks; the skin and subcutaneous melanoma from these animals were also analyzed. Although the B16 tumors are more easily visualized than the GL261 tumors due to their black color, the B16 tumors are more difficult to remove because although some animals have localized tumors, most animals have tumors that tend to spread along the meninges and are less localized than

the GL261 tumors. Figure 3.12 shows a murine brain with intracranial B16 melanoma, and figure 3.13 shows a murine brain with intracranial GL261 glioma tumor. It is clear that not only are the color and growth pattern of the 2 tumors different, the morphology of the tumor cell also looks different, therefore, it is possible that their BPA-f pharmacokinetics may also be different.

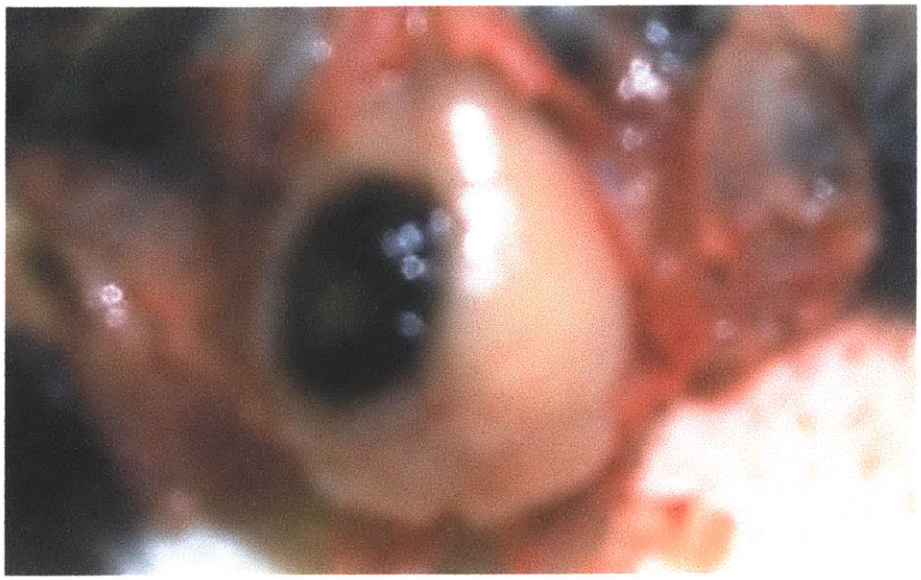

Figure 3.12 Murine Brain with intracranial B16 Melanoma.

Figure 3.13 Intracranial GL261 glioma tumor.

The time dependence of ^{10}B accumulation in intracranial B16 tumor, normal brain tissue, subcutaneous melanoma and skin is shown in figure 3.14, with the ratios shown in figure 3.15. It can be seen that B16 cells quickly take up BPA-f after injection, with the ^{10}B concentration in B16 cells reached up to 8-10 times that of normal brain tissue at 15 minutes after BPA-f injection. Similar to GL261 glioma tumor, both the tumor: blood and tumor: normal brain ^{10}B concentration ratios vary with time, although in this case, the ^{10}B concentration in B16 tumor does not decrease as rapidly as in GL261, the B16 tumor still has 5 times higher ^{10}B concentration than in normal at 240 minutes after injection. At all times, the ^{10}B concentration in B16 tumors is consistently higher than the ^{10}B concentration in normal brain tissues, which is qualitatively consistent with the human GBM biopsy data[22], the human melanoma data[27] and the GL261 glioma tumor model. This difference could be due to the different tumor cell lines with their different metabolism requirements and vascularity. However, this result confirmed again that blood, normal brain and tumor all have quite different BPA-f pharmacokinetics. A detailed knowledge of the pharmacokinetic behaviors of these tissues has practical implications for treatment planning. It is also observed that the subcutaneous melanoma has consistently lower ^{10}B concentration than the intracranial melanoma. One possible explanation could be that there are differences in vascular supplies between the two environments, although there is not sufficient data points to conclude statistically. Additional observations show that for all time points studied, the subcutaneous melanoma ^{10}B concentration is approximately 2 times that of skin, while at 30 minutes after injection, the subcutaneous melanoma is about 3 times of the ^{10}B concentration in skin.

Again, by using the 3-compartment model detailed in section 2.3, and minimizing the sums of the squares of the residues, the rate constants for the compartment-model of BPA-f pharmacokinetics for normal brain and B16 tumor were obtained. The values for k1 through k4 for the normal brains are 0.009 ml/g/min, 0.25 min^{-1}, 0.033 min^{-1} and 0.011 min^{-1}, respectively, which are very close to that observed by Imahori[16] in the human PET studies (0.011 ml/g/min, 0.025 min^{-1}, 0.033 min^{-1} and 0.009 min^{-1}, respectively). The values for k1 through k4 for the B16 intracranial melanoma are 0.262 ml/g/min, 0.211 min^{-1}, 0.058 min^{-1}, and 0.011 min^{-1}. These values differ substantially

from the values Imahori obtained for GBM, which are 0.027 ml/g/min, 0.041 min^{-1}, 0.029min^{-1} and 0.013 min^{-1}, respectively; they also differ from the values obtained from the GL261 tumors, which are 0.178 ml/g/min, 0.181 min^{-1}, 0.091 min^{-1}, and 0.036 min^{-1}, respectively. These results are summarized in table 3.1. The most notable difference between the GL261 and the B16 is the initial influx across the blood-brain-barrier, and the efflux from the intracellular compartment. One possible explanation could be as follows: since BPA-f is an analogue of the melanin precursor, the B16 cells will have more transport carriers on their cell membranes, thereby contributing to the higher influx rate initially. However, it is conceivable that once the precursors get into the cells, they are rapidly converted to melanin and bound inside the cell. Therefore, the efflux from the intracellular compartment will decrease. The results of fitting the B16 experimental data using the k's derived from the 3-compartment model is shown in figure 3.16.

Tissue	k1 (ml/g/min)	k2 (min^{-1})	k3 (min^{-1})	k4 (min^{-1})
GBM (n=6)*	0.027±0.07	0.041±0.018	0.029±0.008	0.013±0.007
GL261 (n=6)	0.178±0.025	0.181±0.037	0.091±0.013	0.036±0.009
B16 (n=6)	0.262±0.042	0.211±0.031	0.058±0.015	0.011±0.006
Normal Brain				
Human (n=16)*	0.011±0.003	0.025±0.010	0.033±0.015	0.009±0.011
GL261 (n=6)	0.010±0.004	0.025±0.009	0.033±0.009	0.011±0.006
B16 (n=6)	0.009±0.003	0.025±0.007	0.033±0.010	0.011±0.003

Table 3.1 k1 through k2 values for GBM[16] , GL261 and B16 tumors

* Data from Imahori PET study[16]

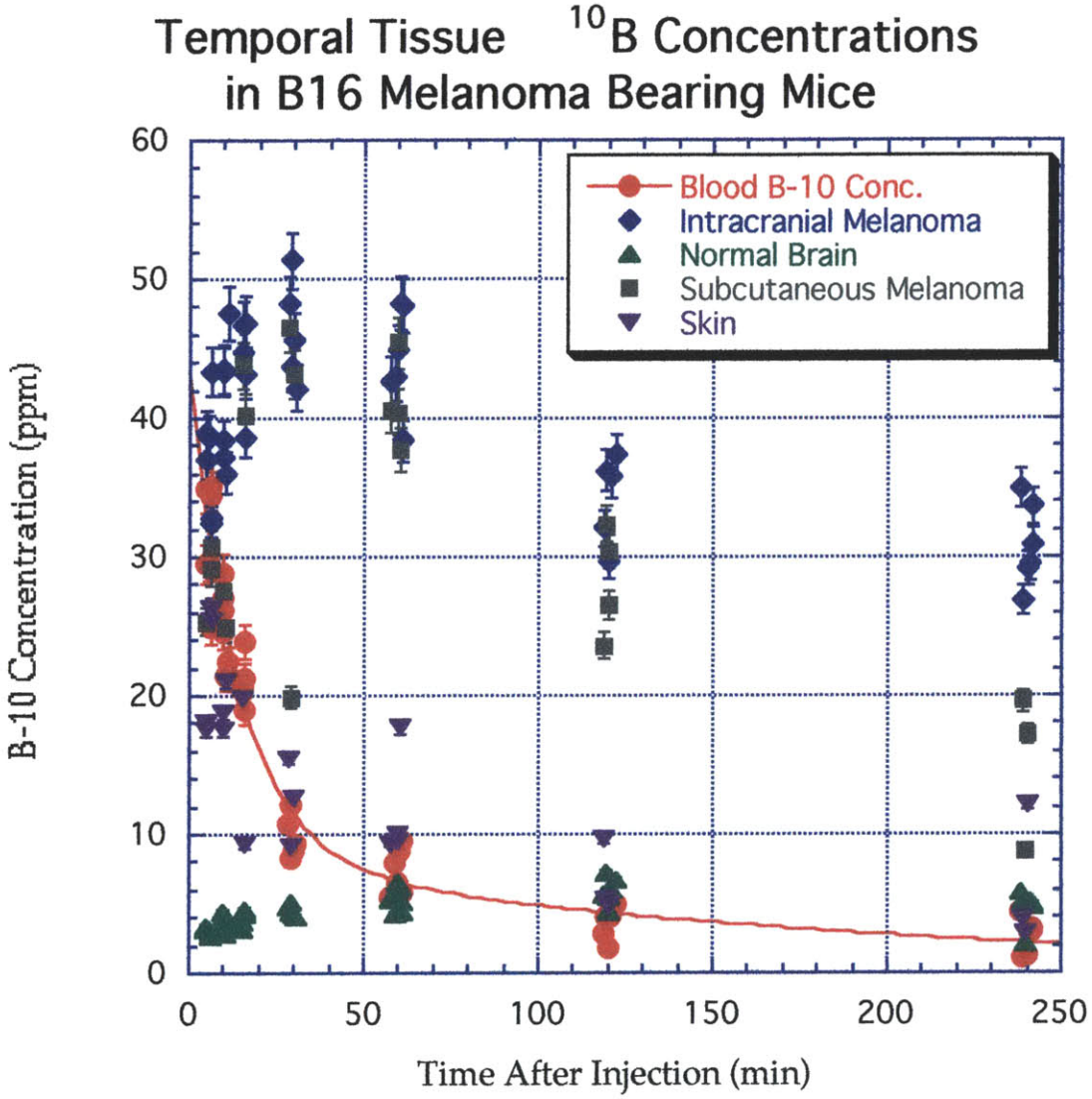

Figure 3.14 ^{10}B concentrations in intracranial B16 melanoma, normal brain, subcutaneous melanoma and skin after a 350 mg BPA-f/kg weight bolus injection

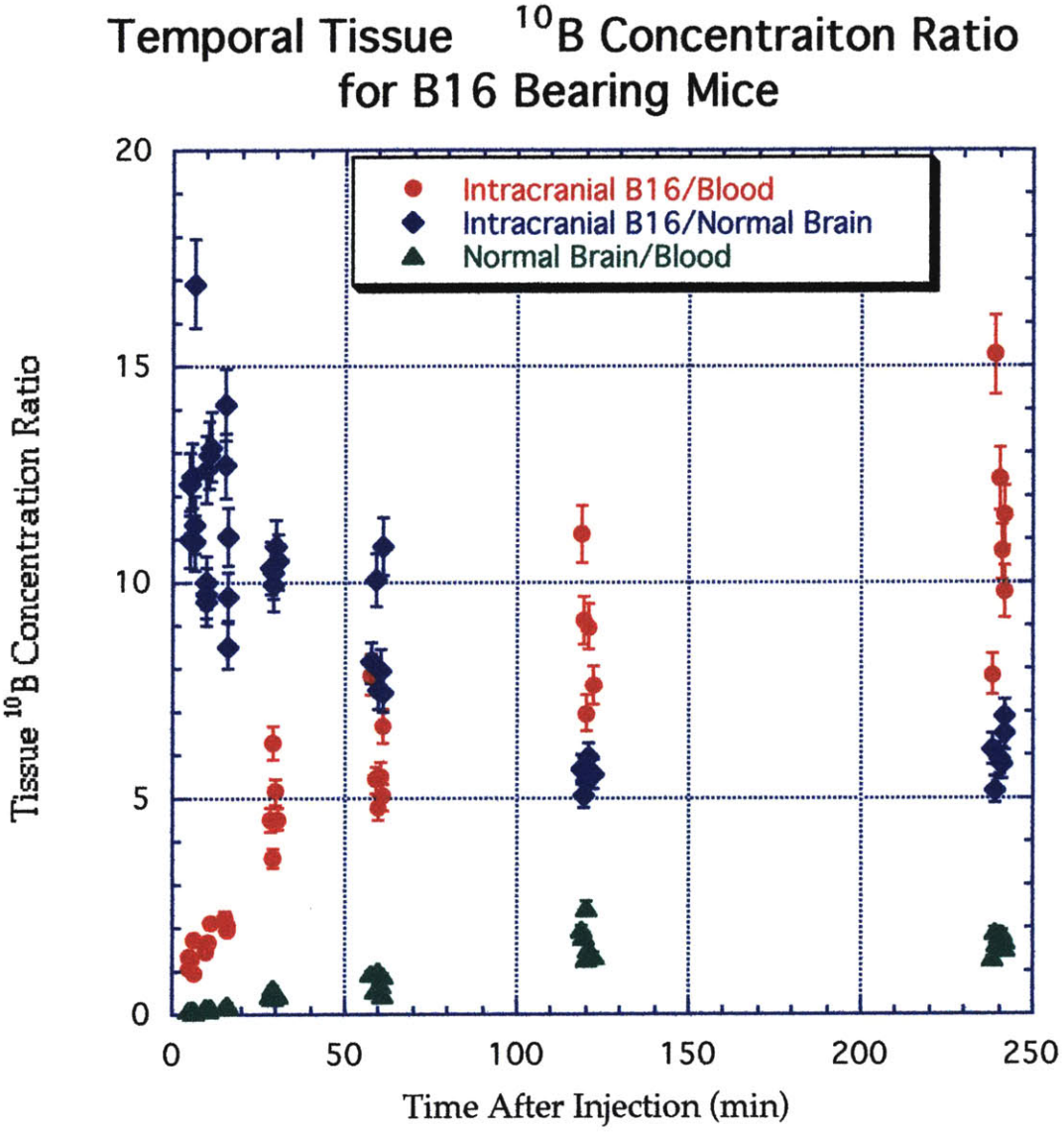

Figure 3.15 ^{10}B Concentration Ratios for Intracranial B16/Blood, Intracranial B16/Normal Brain, and Normal Brain/Blood

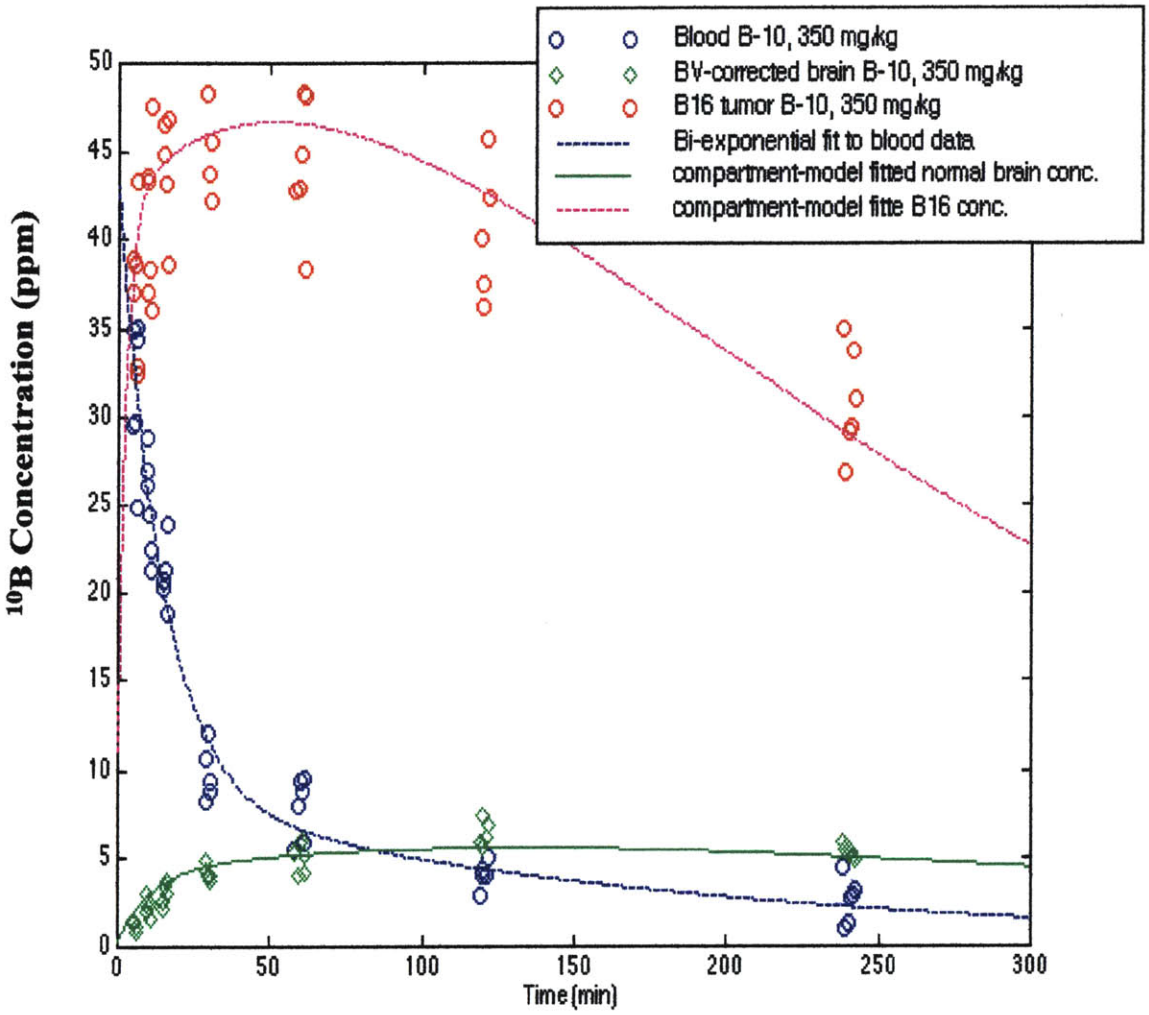

Figure 3.16 Experimental data from averaged B16 intracranial melanoma and normal brain fitted to the 3-compartment model

Figure 3.17 and 3.18 are the predicted ^{10}B concentration ratio between turmor and normal brain, tumor and blood, and normal brain to blood using the three-compartment model and the rate constants derived. It is apparent that the normal to blood ratios for both GL16 and B16 are very similar, while the tumor to blood and tumor to normal brain ratios between the two systems are different. They further demonstrate that for different tumor cell lines, the BPA-f pharmacokinetics is different.

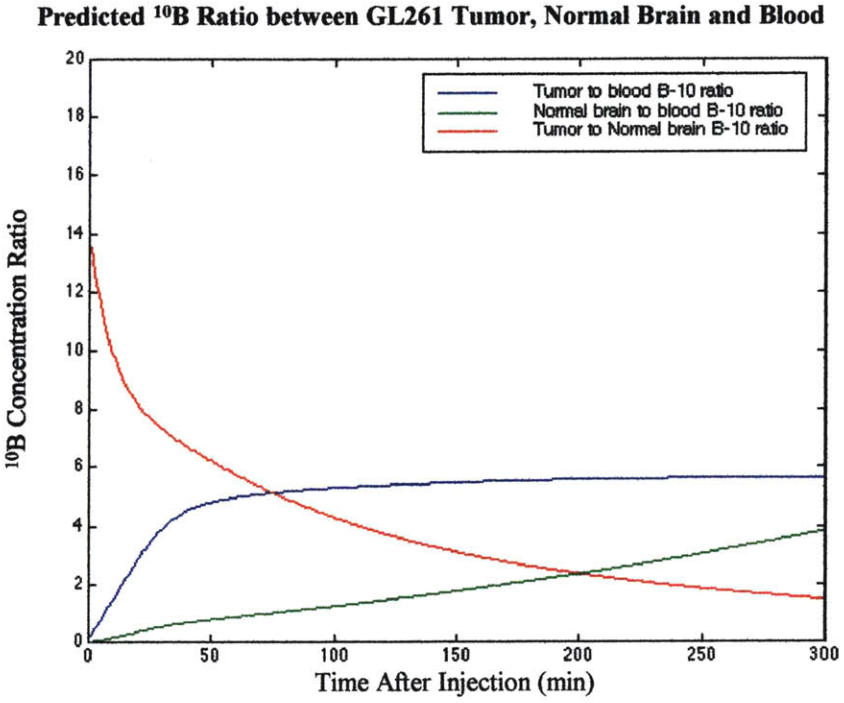

Figure 3.17 Three-compartment model predicted ^{10}B concentration ratio for GL261 tumor

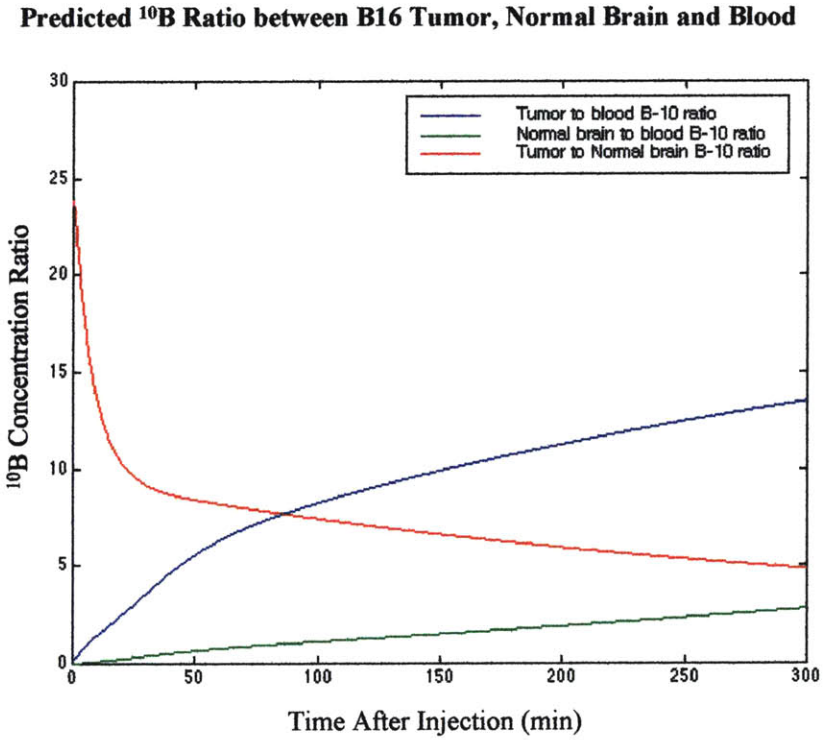

Figure 3.18 Three-compartment model predicted ^{10}B concentration ratio for B16 tumor

3.4 BPA-f Pharmacokinetics study in CX01 Hepatic Colorectal Metastasis

3.4.1 Introduction

In 1998 more than 150,000 Americans will be diagnosed with colorectal cancer, and over 60,000 will die from this tumor. 15 - 25% will have hepatic metastases at the time of diagnosis, and another 20 - 30% will develop metastatic hepatic lesions subsequent to resection of the primary tumor. Treatment options for hepatic metastases include aggressive surgical resection, administration of regional chemotherapeutic agents, systemic chemotherapy, radiotherapy, or other palliative and experimental procedures. Despite well-defined pharmacological benefits of selected chemotherapeutics, there is no convincing survival advantage for many of the above mentioned techniques[28-30]. The median survival after diagnosis is typically 22-24 months, and has changed minimally over the past decade.

Colorectal metastases are hypovascular and can continue to grow under hypoxic conditions. Thus, the use of an actively transported boron-containing compound selectively localized in tumor and the high-LET radiation produced by BNCT could be a useful therapeutic approach to this clinical problem. This approach has previously been considered by the BNCT group at the University of Pavia, in Italy, where animal experiments were conducted using boric acid, sodium borocaptate (BSH), and ^{10}B-conjugated tetraphenyl porphyrin sulfonate (TPPS)[31]. Toxicity and biodistribution studies following intravenous injection of these compounds were performed. More recently, they have conducted an experiment in which diffused hepatic metastases were induced in BD-IX rats, the rats were then given autotransplantation and their livers underwent BNCT procedures[32]. In this experiment, they used BPA-f with a dose of 300 mg BPA/kg weight. The 300-second irradiations occurred 2-3 hours after BPA administration. The tumor to normal liver ratio they detected was 3.9[32].

In the present study, a well-characterized animal model employing the athymic mouse was used to gain information on the biodistribution of Boronophenylalanine-fructose (BPA-f) in hepatic colorectal metastases and normal liver tissue as a function of time. The goal was to investigate whether BPA-f has a preferential uptake in hepatic

colorectal metastasis. If the tumor does possess preferential uptake relative to normal liver, BNCT could be a plausible treatment alternative for the treatment of hepatic colorectal metastasis.

3.4.2 Materials and Methods

The CX-1 hepatic colorectal metastasis model: Tumor cells were grown and harvested in collaboration with the Tumor Biology Lab of the Department of Cancer Biology at the Beth Israel Deaconess Medical Center. The CX-1 is a human colon cancer cell line. The cells are maintained in RPMI 1640 medium (GIBCO Laboratories Life Technologies Inc., Grand Island, NY) with 10% fetal bovine serum (FBS; SIGMA Chemical Company, St. Louis, MO), 1% L-Glutamine (GIBCO), 100 units/ml of penicillin G (GIBCO) and 100 mg/ml streptomycin (GIBCO). For the inoculation of tumor into animals, 10^7 cells/ml phosphate buffered saline at pH 7.4 is used

Generation of Hepatic Tumor: For the initiation of hepatic tumors, 10 week old female athymic nude mice (Taconic, Germantown, NY) were first anesthetized (intraperitoneal injection of Pentobarbital, 30 mg/kg body weight), and a small left subcostal incision was made. After gently teasing the spleen out using a pair of tweezers, 0.1 ml of the cell suspension (10^7 cells/ml phosphate buffered saline in pH 7.4) was injected into the spleen of the mouse using a 26-gauge needle. Due to the fact that the spleen shares blood supply with the liver, intrasplenic injection of tumor cells will result in multiple hypovascular metastases which will be well established 6 weeks after implantation. The tumor take rate is ~80%.

Experimental Procedures: Thirty five 16 week old female athymic nude mice bearing hepatic colorectal metastases were given a bolus injection of BPA-f (350 mg BPA-f/kg body weight) through the tail vein using a 26G needle. This is the same dose as is currently being used in the Harvard-MIT BNCT clinical trial. Five mice were sacrificed at each of the 7 different time points (5, 10, 15, 30, 60, 120, and 240 minutes after injection). Cardiac puncture was performed to collect blood samples. Samples of

skin, tumor and normal liver tissues were removed after the death of the animal. The blood ^{10}B concentration was analyzed using PGNAA, while the tissues were first acid digested, then analyzed for their ^{10}B concentrations using ICP-AES.

3.4.3 Results and Discussion

Thirty five athymic nude mice bearing hepatic colorectal metastasis were used for the BPA-f biodistribution studies. Most mice had multiple metastatic nodules while a few had more than half of their livers replaced by tumor. They all received a bolus injection of BPA-f (350 mg BPA-f /kg body weight) through the tail vein. They were separated into 7 groups and sacrificed at the prescribed time points (5, 10, 15, 30, 60, 120, and 240 min after injection). Blood samples were drawn at sacrifice and analyzed using PGNAA. Samples of skin, normal liver, and tumor were collected after death and were analyzed by ICP-AES after acid-digestion. Figure 3.19 shows the time dependence of boron accumulation in blood, skin, normal liver, and tumor. It is clear that both the skin and the normal liver follow a similar time course as the blood, which is to be expected since they are both highly vascularized organs. It was speculated that due to the hypovascular nature of the hepatic colorectal metastasis, the boron accumulation in the tumor lagged behind that of the normal liver, but quickly built up and surpassed that of the normal liver. From figure 3.20, it is shown that at 15 min after the bolus injection the metastases had 1.5 times the boron concentration in blood, increasing to approximately 2.5 times by 60 min after injection, and decreasing again to about 1.5 times at 240 min. Similar trends were observed for tumor/normal liver, and tumor/skin. Tumor boron was approximately 1.3 times that in normal liver at 15 min, 1.8 times at 30 min, 2 times at 60 min and 120 min, and barely 1 at 240 min after the bolus injection. However, the skin shows consistent higher ^{10}B concentration than the blood, and since it is the first organ to be penetrated by the neutron beam for liver irradiation, it might be important to examine the effect of the elevated ^{10}B concentration in the skin.

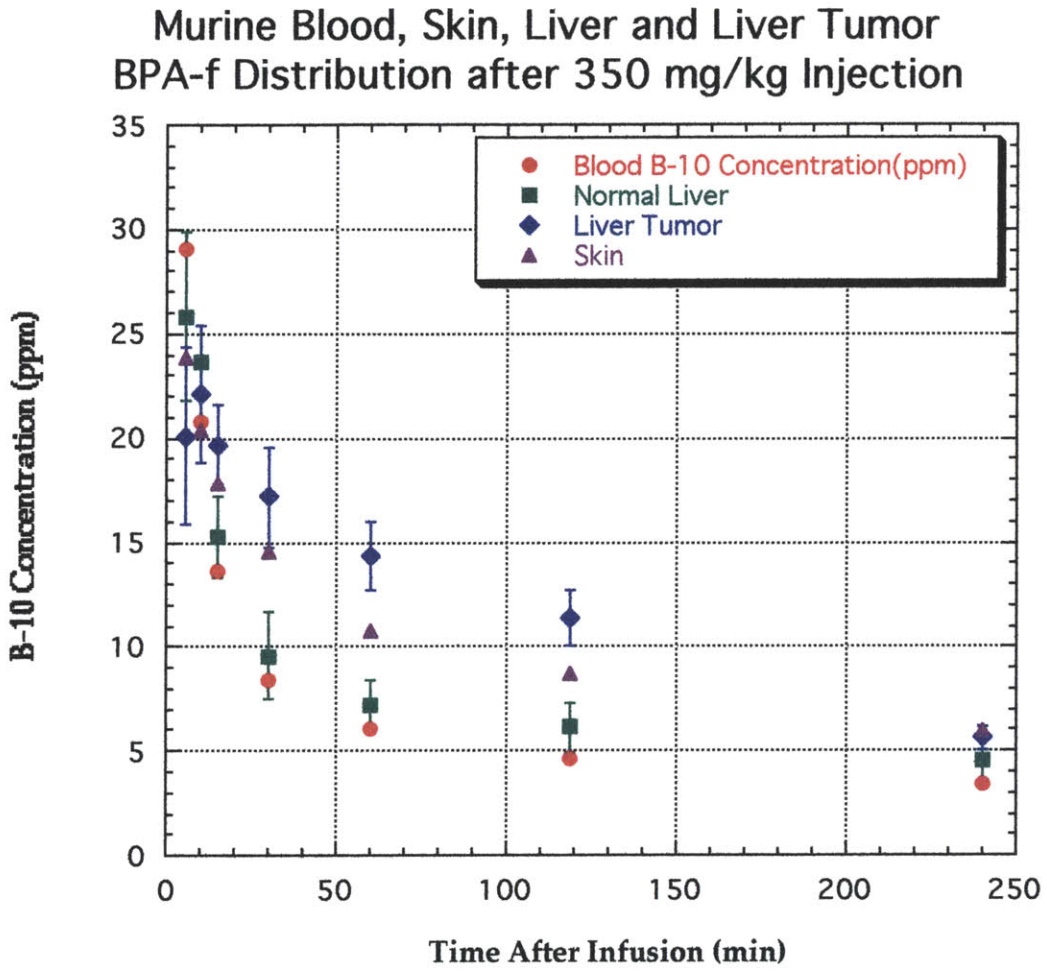

Figure 3.19 ^{10}B biodistribution in blood, normal liver, hepatic colorectal metastasis and skin.

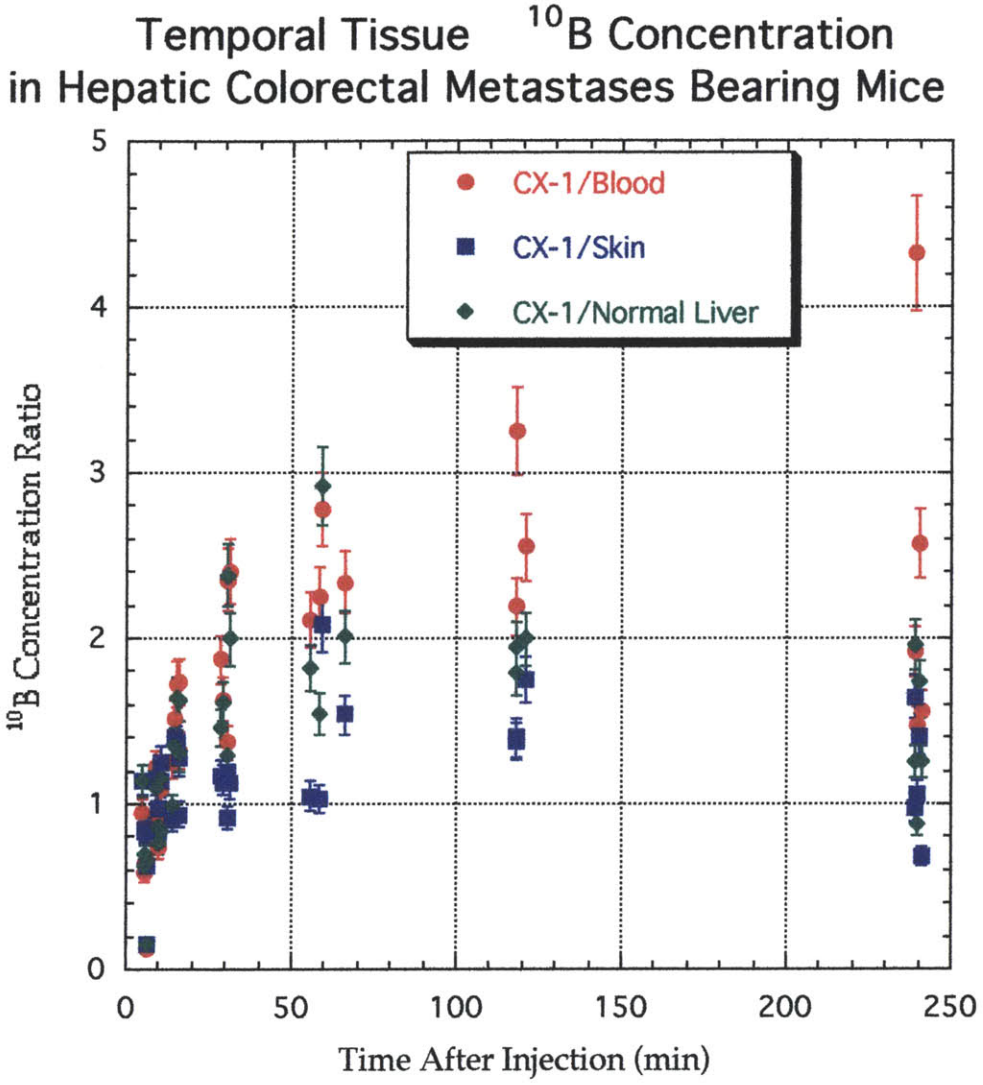

Figure 3.20 ^{10}B biodistribution ratio for CX-1/blood, CX-1/normal liver, CX-1/Skin, Normal Liver/Blood, and Skin/Blood.

Calculations were carried out to quickly estimate significance of an elevated skin ^{10}B concentration. Due to the unavailability of a realistic liver/body model, the ellipsoidal head phantom was used. The FCB dose profile in the ellipsoidal head phantom was used in the calculations[15], the skin was assumed to span from 0 to 1 cm and the liver from 2 cm to the edge of the phantom, with the higher ^{10}B concentration employed for skin (27 ppm) and tumor (35.4 ppm). Since there are no RBE values available for liver, the brain RBE values were used. Figure 3.21 shows the dose profile

calculated in the head phantom. It appears that with the ^{10}B concentration ratio achieved and the high skin ^{10}B concentration present, significant dose will be delivered to the skin even with the deep penetrating FCB.

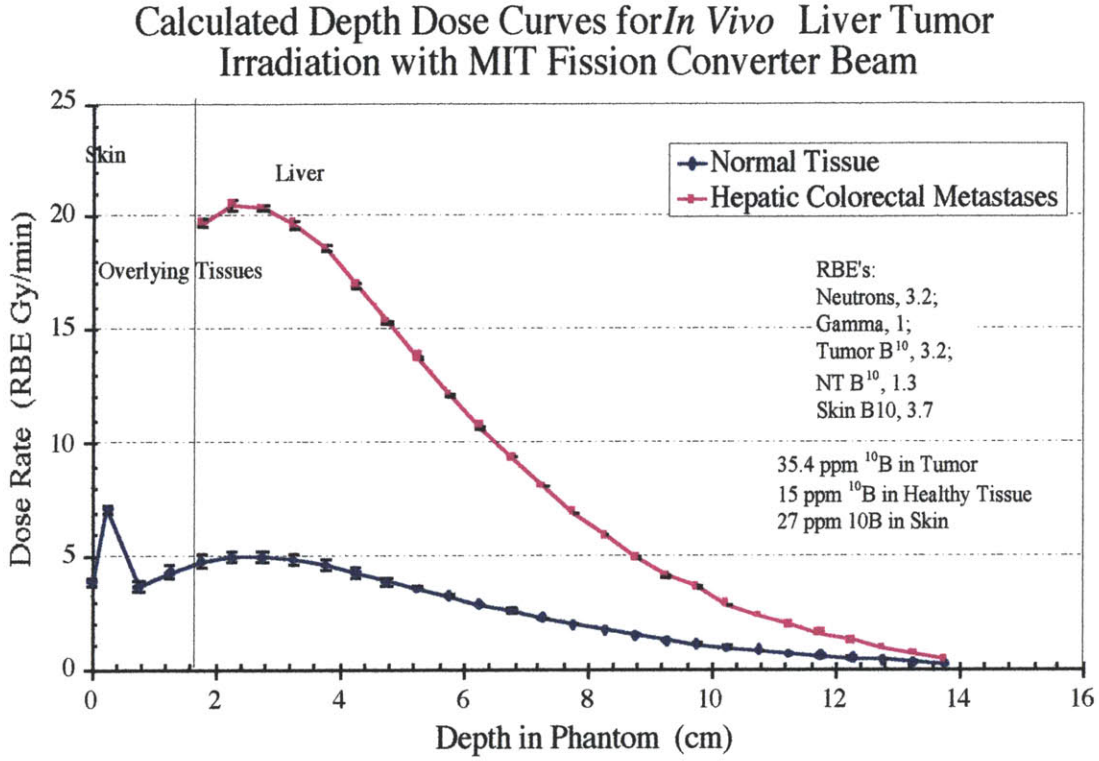

Figure 3.21 Liver Dose Rate Profile from Fission Converter Neutron Beam[15]

Figure 3.22 and 3.23 are H & E stained histological sections of normal liver and hepatic colorectal metastasis to demonstrate the different morphology of the two tissues.

In summary, to obtain a tumor therapeutric ratio of greater than unity in liver, a highly vascularized organ, represents a challenge for BNCT. Nevertheless, in the present study encouraging results for BPA-f uptake in hepatic colorectal metastases were obtained. In the athymic mouse model, during 30 - 60 min after a bolus injection, the differential uptake of BPA-f in the hepatic metastases and normal liver tissue was approximately equal to 2 (T/NT). While this ratio is lower than that seen in experimental brain tumor models, it is encouraging given the biology of this setting. The problem seems to lie in the fact that skin also has higher ^{10}B concentration than blood or normal liver, therefore, the dose received by the skin may be high and become the limiting organ

for toxicity. Additional research will have to be conducted to derive the RBEs for the liver and the hepatic colorectal metastases. Once obtained, it will be possible to generate detailed dosimetric calculations using realistic liver/body model, and to determine the suitability of BNCT for the treatment of hepatic colorectal metastasis.

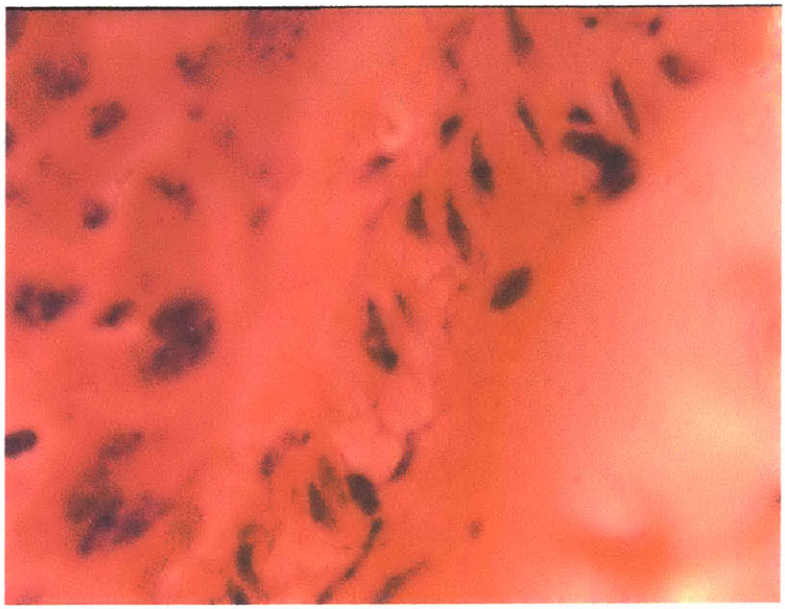

Figure 3.22 H & E stained histological section of normal liver tissue next to a capillary.

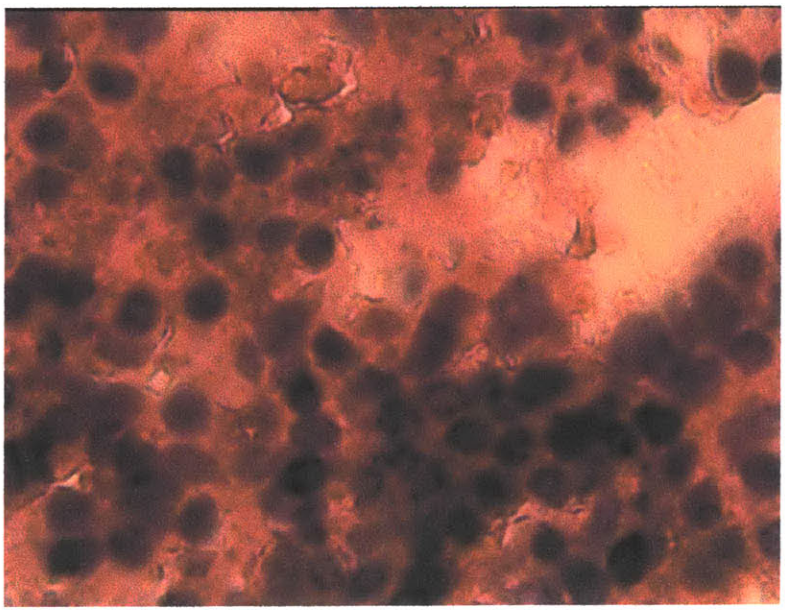

Figure 3.23 H & E stained histological section of hepatic colorectal metastasis.

3.5 Lung ^{10}B Measurements

The M67 beam currently used in the Harvard-MIT BNCT Phase I clinical trial is a vertical beam, and the subjects are sometimes positioned with their torso in close proximity to the beam. Since the M67 beam has considerable fast neutron contamination, with this kind of positioning it is conceivable that some radiation damage might occur if BPA-f uptake is significant in either the heart or the lungs. This issue becomes increasingly important as stepwise dose escalation has prolonged the total irradiation time to 400 - 600 minutes. Therefore, an investigation into the BPA-f uptake in lungs was initiated.

Lung samples from the GL261 murine glioma model study mice were collected after they were sacrificed. These lung samples were collected in anticipation of a possible study of lung dose, they were weighed, then stored in a –70° freezer in tightly sealed eppendorf tubes. It was decided that the issue was important enough to warrant a closer look. The samples were first acid-digested and analyzed for their ^{10}B concentrations using ICP-AES. The lung ^{10}B concentrations were found to be 8-10 times higher than the normal brain ^{10}B concentrations during the late time periods (30-240 minutes after 350 mg BPA-f/kg weight bolus injection). More significantly, the ^{10}B concentrations in lungs do not seem to decrease with time. Figure 3.24 shows the results of these lung samples.

The results were of such an extreme nature that verifications are required. The issue of contamination was ruled out by measuring the ^{10}B concentration of the nitric acid-sulfuric acid mixture and the Triton X-100 solutions used for acid-digestion. PGNAA measurements showed that neither solution contained ^{10}B.

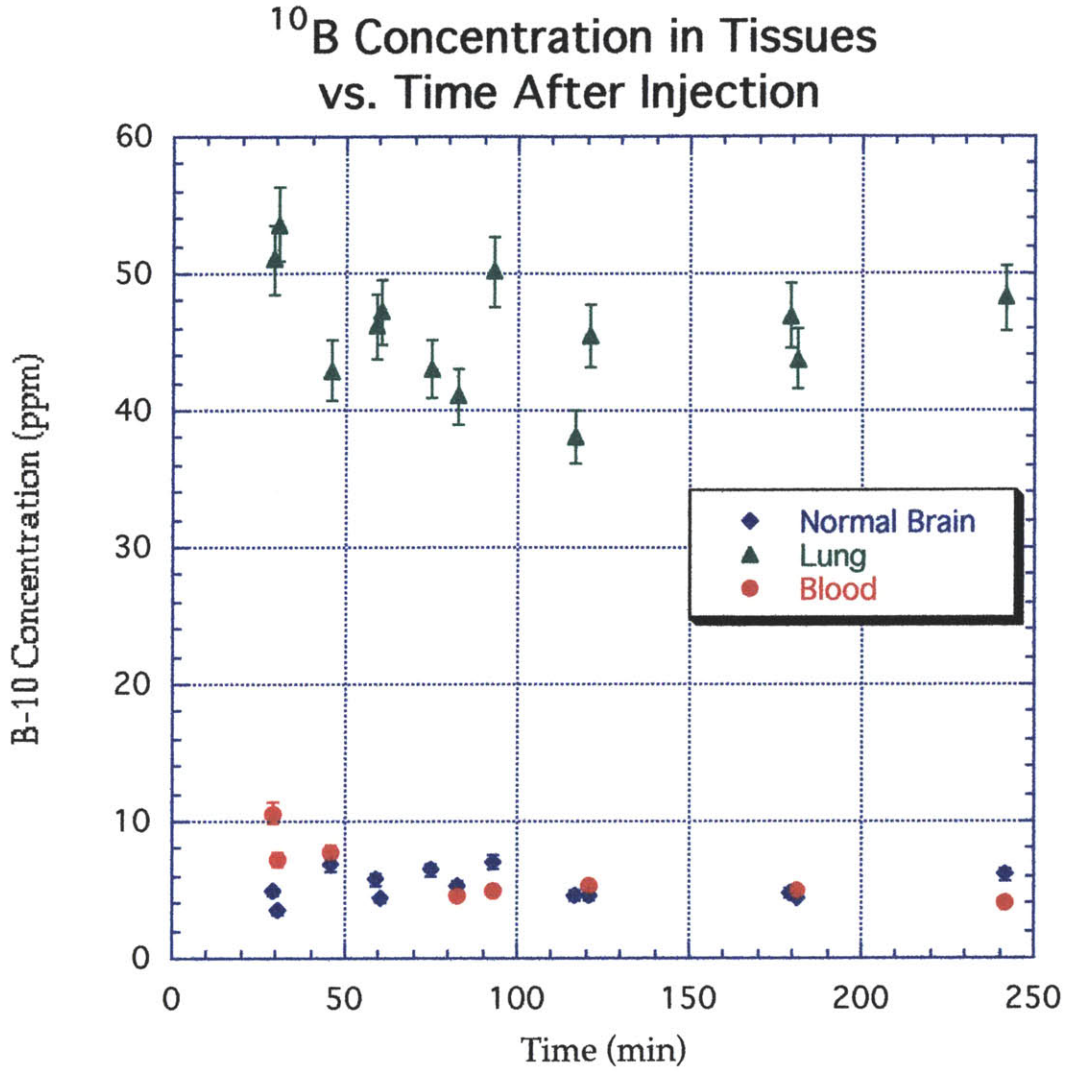

Figure 3.24 ^{10}B concentrations in blood, normal brain and lung tissue in GL261 bearing mice.

It was decided that a verification of the data was required. The animal study being studied at this time was the B16 intracranial melanoma model. Four lung samples were collected and measured using PGNAA. Table 3.2 shows the results of the PGNAA measurements.

It is worth noting that a calibration curve using only 0.05 ml of standards was used for this measurement because the tissue samples were too small. By using approximately the correct volume for standards, the ^{10}B concentrations obtained using

either the B/H method or using only the B peak count rates give similar results (table 2.2), with a maximum difference of 30%. Although these results still showed that lung tissues did have higher ^{10}B concentrations than blood and normal brain tissues, the factor is only 4 – 5 times higher instead of 8 –10 as measured by ICP-AES.

Sample #	Sample Weight	Time (min)	^{10}B Concentration
11	48.3 mg	9.5	29.8 ± 2.2 ppm
15	52.4 mg	16	23.2 ± 1.7 ppm
32	37.9 mg	60	19.4 ± 1.4 ppm
31	48.4 mg	30	19.7 ± 1.9 ppm

Table 3.2 PGNAA ^{10}B measurements of lung tissues

To resolve the discrepancy between the lung ^{10}B concentrations measured by ICP-AES and that measured by PGNAA, another experiment was conducted. Since by this time, there were no longer mice available that were carrying intracranial tumors, four healthy mice were given bolus injections of 350 mg BPA-f/kg weight through their tail veins. They were sacrificed at different time points, and their lungs were removed. The results were shown in Table 2.3 in chapter 2 under PGNAA and ICP-AES intercomparison. It reveals that for healthy mice, the lung ^{10}B concentrations follow the blood curve, with higher ^{10}B concentrations for earlier time points and low ^{10}B concentrations for later time points.

It is apparent that there is no error in the lung ^{10}B concentration measurements obtained by ICP-AES or by PGNAA. The apparent discrepancy in the ^{10}B concentrations is most likely due to the health of the animals. For healthy mice, the ^{10}B concentration in the lungs appear to follow the blood pharmacokinetics and is approximately the same as in the blood (with the exception of the early time point at 6 minutes). However, for mice with intracranial tumors, the lung ^{10}B concentrations do not seem to follow the blood distribution. For mice with B16 intracranial melanoma, with a lung ^{10}B concentration approximately the same as blood, is 8 times that of the normal brain, as seen at the 10 minute time point. At the 60 minute time point, the lung ^{10}B concentration is twice as

high as the blood, but 4 times the ^{10}B concentration in normal brain. The pattern might be very different for a much later time point, such as 240 minutes after injection. For mice with GL261 glioma tumor, only later time points were sampled so that no observations are available for the earlier times. However, for the 30 minutes time points, the lung ^{10}B concentration is approximately 5-7 times of that seen in the blood, and approximately 8-10 times of normal brain; for 240 minutes samples, the lung ^{10}B concentration is approximately 10 times higher than normal brain and blood. Tumor bearing mice are smaller in size (14 g to 16 g as opposed to 22 g for healthy mice) and more lethargic than healthy mice and are likely to have decreased food intake. No explanation could be suggested for the lung ^{10}B concentration difference, since the experimental conditions were similar, with the only difference being the health status of the animals.

3.6 References

1. Kiger III, W.S., S. Sakamoto, and O.K. Harling, *Neutronic Design of A Fission Converter-Based Epithermal Neutron Beam for Neutron Capture Therapy.* Nuclear Science and Engineering, 1999. **131**: p. 1-22.

2. Morris, G.M., *et al.*, *Response of the central nervous system to boron neutron capture irradiation: evaluation using rat spinal cord model.* Radiother Oncol, 1994. **32**: p. 249-255.

3. Coderre, J.A., *et al.*, *Comparative Assessment of Single-Dose and Fractionated Boron Neutron Capture Therapy.* Radiat Res, 1995. **144**(3): p. 310-7.

4. Morris, G.M., *et al.*, *Central nervous system tolerance to boron neutron capture therapy with p-boronophenylalanine.* British Journal of Cancer, 1997. **76**: p. 1623-1629.

5. Morris, G.M., *et al.*, *Boron neutron capture irradiation of the rat spinal cord: effects of variable doses of borocaptate sodium.* Radiother Oncol, 1996. **39**(3): p. 253-9.

6. Morris, G.M., *et al.*, *Response of the central nervous system to fractionated boron neutron capture irradiation: studies with borocaptate sodium.* Int J Radiat Biol, 1997. **71**(2): p. 185-92.

7. Gavin, P.R., *et al.*, *Large animal normal tissue tolerance using an epithermal neutron beam and borocaptate sodium.* Strahlenther Onkol, 1993. **169**(1): p. 48-56.

8. Gavin, P.R., *et al.*, *Large animal normal tissue tolerance with boron neutron capture.* Int J Radiat Oncol Biol Phys, 1994. **28**(5): p. 1099-106.

9. Huiskamp, R., *et al.*, *Brain tolerance in dogs to boron neutron capture therapy with borocaptate sodium (BSH) or borophenylalanine (BPA)*, in *Cancer Neutron Capture Therapy*, Y. Mishima, Editor. 1996, Plenum Press: New York. p. 591-598.

10. Hawkins, R.A., A.M. Mans, and J.F. Biebuyck, *Amino Acid Supply to Individual Cerebral Structures in Awake and Anesthetized Rats.* American Journal of Physiology, 1982. **242**: p. E1-E11.

11. Craigie, E.H., *On the relative vascularity of various parts of the central nervous system of the albino rat.* Journal of Comparative Neurology, 1920. **31**: p. 429-464.

12. Kiger III, W.S., *et al. A Pharmacokinetic Model for the Concentration of Boron-10 in Blood following BPA-f Administration in Humans.* in *Eighth International*

Conference on Neutron Capture Therapy for Cancer. 1998. LaJolla, CA: Plenum Press.

13. Coderre, J.A., *et al.*, *Boron neutron capture therapy of glioblastoma multiforme using the p-boronophenylalanine-fructose complex and epithermal neutrons: Trial design and early clinical results.* Journal of Neuro-Oncology, 1997. **33**: p. 141-152.

14. Zamenhof, R.G., *et al.*, *MacNCTPLAN: An improved Macintosh-based treatment planning program for boron neutron capture therapy.*, in *Advances in Neutron Capture Therapy*, B. Larsson, J. Crawford, and R. Weinreich, Editors. 1997, Elsevier: Amsterdam. p. 100-105.

15. Kiger III, W.S., *Personal Communications.* .

16. Imahori, Y., *et al.*, *Fluorine-18-labeled fluoroboronophenylalanine PET in patients with glioma.* Journal of Nuclear Medicine, 1998. **39**: p. 325-333.

17. Coderre, J.A., *et al.*, *Application of BNCT to other types of tumors.*, in *Advances in Neutron Capture Therapy*, B. Larsson, J. Crawford, and R. Weinreich, Editors. 1997, Elsevier: Amsterdam. p. 649-653.

18. Coderre, J.A., *et al.*, *Boron Neutron Capture Therapy of a Murine Melanoma with p-Boronophenylalanine: Dose-Response Analysis using a Morbidity Index.* Radiat Res, 1991. **128**(2): p. 177-85.

19. Coderre, J.A., *et al.*, *Selective Delivery of Boron by the Melanin Precursor Analogue p-Boronophenylalanine to Tumors Other Than Melanoma.* Phys Med Biol, 1989. **34**(9): p. 1301-7.

20. Solares, G., *et al.*, *Biodistribution and Pharmacokinetics of p-Borono-phenylalanine in C57BL/6 Mice with GL261 Intracerebral Tumors, and Survival Following Neutron Capture Therapy*, in Progress in Neutron Capture Therapy for Cancer, D.E.M.B.J.A.B.V. Harrington, Editor. 1992, Plenum Press: New York and London. p. 475-478.

21. Saris, S.C., *et al.*, *Boron neutron capture therapy for murine malignant gliomas.* Cancer Res, 1992. **52**(17): p. 4672-4677.

22. Coderre, J.A., *et al.*, *Biodistribution of Boronophenylalanine in Patients with Glioblastoma Multiforme: Boron Concentration Correlates with Tumor Cellularity.* Radiation Research, 1998. **149**: p. 163-170.

23. Busse, P.M., *et al. The Harvard-MIT BNCT program: overview of the clinical trials and translational research.* in *Eighth International Conference on Neutron Capture Therapy for Cancer*. 1998. LaJolla, CA: Plenum Press.

24. Busse, P.M., *et al.*, *Clinical follow-up of patients with melanoma of the extremity treated in a phase I boron neutron capture therapy protocol.*, in *Advances in Neutron Capture Therapy*, B. Larsson, J. Crawford, and R. Weinreich, Editors. 1997, Elsevier: Amsterdam. p. 60-64.

25. Fukuda, H., *et al.*, *Boron neutron capture therapy of malignant melanoma using ^{10}B-paraboronophenylalanine with special reference to evaluation of radiation dose and damage to the skin.* Radiation Research, 1994. **138**: p. 435-442.

26. Mishima, Y., *Melanogenesis investigation leading to selective melanoma neutron capture therapy and diagnosis.* J Dermatol, 1994. **21**(11): p. 907-14.

27. Mishima, Y. *Current clinical paradigms in melanoma BNCT.* in *Eighth International Conference on Neutron Capture Therapy for Cancer*. 1998. LaJolla: Plenum Press.

28. Hanazaki, K., *et al.*, *Carcinoembryonic antigen and intra-arterial chemotherapy response of liver metastases.* Hepatogastroenterology, 1998. **45**(20): p. 462-467.

29. O'Connell, M., *et al.*, *Sequential intrahepatic flurodeoxyuridine and systemic fluorouracil plus leucovorin for the treatment of metastatic colorectal cancer confined to the liver.* Journal of Clinical Oncology, 1998. **16**(7): p. 2528-2533.

30. Hill, B., T. Minard, and L. Brady, *Monoclonal antibodies in the treatment of metastatic carcinoma to the liver: updated report of a pilot study including leukapheresis.* American Journal of Clinical Oncology, 1998. **21**(3): p. 291-293.

31. Chiaraviglio, D.e.a., *Feasibility Study of Boron Neutron Capture Therapy for Inoperable Liver Cancers*, in *Progress in Neutron Capture Therapy*, B.J. Allen, D.E. Moore, and B.V. Harrington, Editors. 1992, Plenum Press: New York. p. 497-500.

32. Zonta, A., *et al. Effects of BNCT On Liver Metastases Of Colon Adenocarcinoma. A Microscopic and Ultrastructural Study In The Rat.* in *Eighth International Symposium on Neutron Capture Therapy for Cancer*. 1998. La Jolla, CA: Plenum Press.

Chapter 4

Conclusions and Recommendations for Future Work

4.1 Conclusions and Discussion

From the experimental data presented in chapter 3, several observations can be made regarding BPA-f pharmacokinetics. From the first set of experiments on normal brain tissue, the conclusions are presented below:

(1) Within the current dose administration regimen, i.e. 250 – 350 mg BPA-f/kg body weight there exists a linear relationship between the amount of BPA-f administered and the ^{10}B concentrations measured in blood and normal brain tissues. This linearity has also been observed in human Glioblastoma biodistribution experiments albeit at lower infusion concentrations[1]. Therefore, it is anticipated that a higher BPA-f dose would result in a higher ^{10}B concentration in tumor, resulting in a higher tumor radiation dose.

(2) There appear to be slight variations in the spatial BPA-f biodistribution in normal brain tissues. While the right cerebrum, the left cerebrum and the brainstem all have similar ^{10}B concentrations, the cerebellum and the intracranial nerve consistently have higher ^{10}B concentrations throughout the time course studied. These regional variations have also been observed in related neutral amino acids tyrosine and phenylalanine where influxes differ in different brain structures[2].

Although the isodose contours produced using MacNCTPlan showed only small effects, with the uncertainty in the RBEs used, the higher ^{10}B concentration in the intercranial nerve could still have practical dosimetric and treatment planning implications, particularly as higher doses are reached. The result should be verified using a larger animal model with higher spatial resolution. HRQAR experiments could also be employed to determine ^{10}B concentrations and microdosimetry in the intracranial nerves, which are essential to the sensory systems such as sight and hearing.

(3) When the rate constants derived from a human PET glioblastoma study[3] are used in conjunction with blood data from mice to predict the normal brain tissue ^{10}B concentrations in mice, the experimental normal brain data fit very well with the prediction. This suggests that human and mouse have similar BPA-f metabolism and

pharmacokinetics in normal brain tissues, and supports the applicability of the three-compartment model and associated rate constants.

One implication from conclusion number 3 is that ^{10}B is transported into the normal brain in the form of BPA. In the mouse normal brain, only the amount of ^{10}B in the tissues is measured, while in the PET study, it is the ^{18}F that is detected. Neither measurement can independently provide any information on the chemical form of the substance being measured. However, since both ^{10}B and ^{18}F are covalently bound to the phenylalanine ring, it is very likely that they are both transported into the normal brain tissue as the BPA parent. Due to the similar chemical structures of the two, the rate constants are also very similar. This leads to the accurate prediction of mouse normal brain ^{10}B concentrations by the rate constants obtained from ^{18}F-BPA PET study.

From the experiments with the GL261 murine glioma tumor and the B16 intracranial melanoma, it is shown that tumor ^{10}B biodistribution exhibits a different pattern for different tumor lines. The observations are as follows:

(1) GL261 tumor cells take up BPA-f very rapidly, with the ^{10}B concentration of GL261 cells being approximately 7 times of the ^{10}B concentration in normal brain just 30 minutes after bolus injection. However, the ^{10}B concentration in GL261 cells also decreases rapidly, so that by 240 minutes after injection, it is only approximately 2 times the ^{10}B concentration in normal brain. Both the tumor to normal brain ratio and the tumor to blood ratio vary in time.

For GL261 glioma tumor, the optimal time for neutron irradiation may be approximately 60 minutes after the bolus injection, a relatively narrow window. During this time, both the tumor to normal brain and tumor to blood ratio are similar, and are about 6. Since it is not known whether the source of BNCT-induced injury to normal brain is due to vascular or parenchymal damage, this time, 60 minutes, represents the most conservative approach.

(2) The B16 cells also takes up BPA-f rapidly, with the tumor ^{10}B concentration reaching approximately 8 – 10 times that of the normal brain tissue at 30 minutes after injection. However, the ^{10}B concentration decreases much more slowly in the B16 cells. By 240 minutes after injection, B16 cells still possess 5 – 6 times ^{10}B concentration than in the normal brain.

Since the tumor ^{10}B concentration decreases less rapidly in B16 tumors, the neutron irradiation could be performed during the time frame between shortly before 60 minutes to approximately 70 or 80 minutes after the bolus injection. Since the ^{10}B concentrations of brain tissue and of blood cross over between 80 to 100 minutes after injection, the tumor to normal tissue and the tumor to blood ^{10}B concentration ratio will change in the opposite directions during the time frame between 60 – 80 minutes. The actual target tissue for normal brain radiation damages will determine which time point is better suited for neutron irradiation, this issue is clearly demonstrated in figure 4.1.

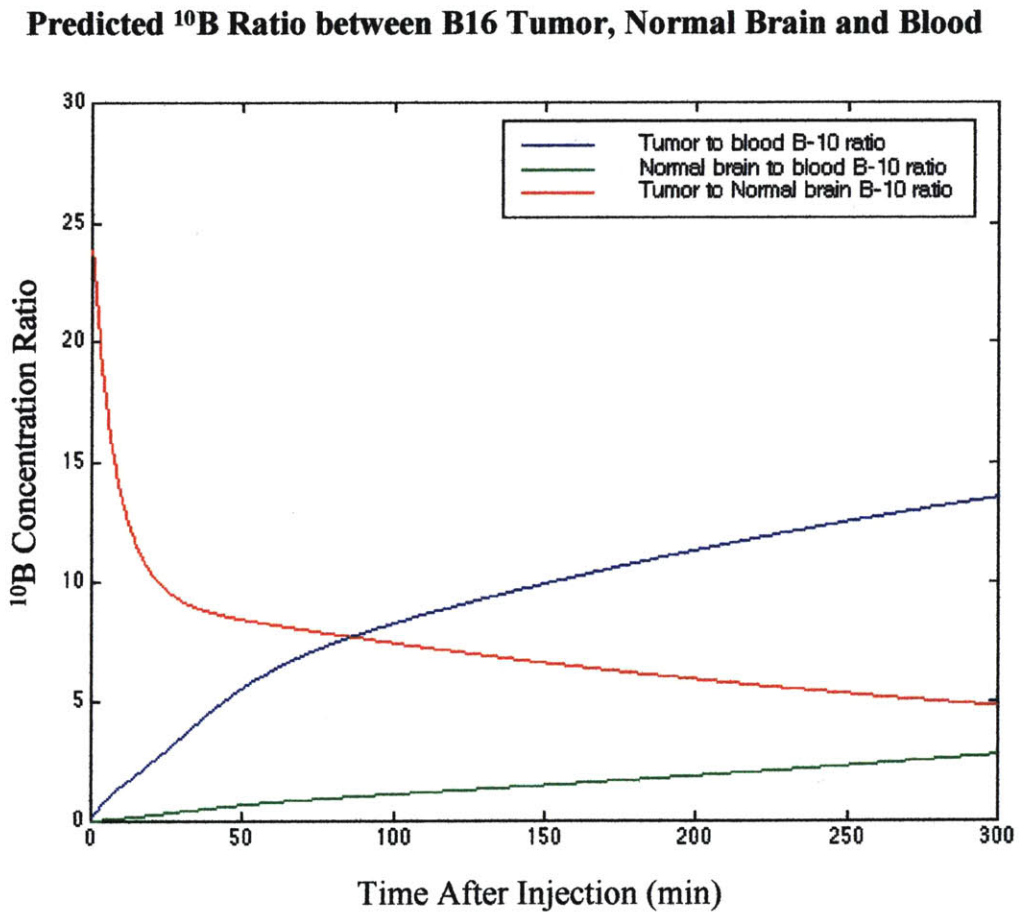

Figure 4.1 Predicted ^{10}B concentration for B16/blood, B16/normal brain and normal brain/blood.

(3) For GL261 tumors, the rate constants k1 through k4 obtained from three-compartment pharmacokinetic model are 0.14 ml/g/min, 0.12 min^{-1}, 0.08 min^{-1}, and 0.036 min^{-1}, respectively.

(4) For B16 intracranial melanoma, the values k1 through k4 are 0.22 ml/g/min, 0.19 min^{-1}, 0.058 min^{-1}, and 0.011min^{-1}.

The rate constants of both tumor models differ substantially from the values Imahori obtained for GBM, which are 0.027 ml/g/min, 0.041 min^{-1}, 0.029 $min^{-1}$and 0.013 min^{-1}, respectively. As mentioned in section 3.3.3, the most notable differences between the GL261 and the B16 are the initial influx across the blood-brain-barrier, and the efflux from the intracellular compartment. A plausible hypothesis is as follows: BPA-f is an analogue of a melanin precursor and B16 cells have more transport carriers on their cell membranes, therefore contributing to the higher influx rate initially. However, it is conceivable that once the precursors get into the cells, they become associated with but not assimilated into melanin as suggested by Mishima[4]. Therefore, the efflux from the intracellular compartment decreases for B16 cells.

From the B16 intracranial melanoma study, two additional conclusions can be made:

(5) intracranial melanoma has higher ^{10}B concentrations than subcutaneous melanoma. This may due to the difference in vascular supply to the tumors.

(6) For all time points studied, the subcutaneous melanoma ^{10}B concentration is at least approximately 2 times that of skin, while at 30 minutes after injection, the subcutaneous melanoma is about 3 times of the ^{10}B concentration in skin.

These studies show that for different tumor cell lines, there are differences in BPA-f pharmacokinetics and that the same cell line grown in different sites can also exhibit different kinetics. The rate constants derived from the pharmacokinetic compartmental vary widely, which could affect the timing of the irradiation. While animal tumor models might not be accurate in predicting the pharmacokinetics of human tumors, they can provide insightful information regarding the pharmacokinetics and perhaps the transport mechanism of BPA-f, thus providing ideas for transport manipulation. In addition, animal models are amenable to further experimentation with irradiation at various times after BPA infusion. Clearly, however, the best way to

determine the optimal irradiation time for human subjects is to study BPA-f pharmacokinetics in humans.

The last experiment was concerned with the ^{10}B biodistribution in hepatic colorectal metastases. Several observations have been made:

(1) Due to the hypovascular nature of hepatic colorectal metastases, the boron accumulation in the tumor lagged behind that of the normal liver, but quickly rose and surpassed that of the normal liver. By 15 min after the bolus injection the metastases had 1.5 times the boron concentration in blood, increasing to approximately 2.5 times by 60 min after injection, and decreasing again to about 1.5 times at 240 min. Similar trends were observed for tumor/normal liver, and tumor/skin. Tumor boron was approximately 1.3 times that in normal liver at 15 min, 1.8 times at 30 min, 2 times at 60 min and 120 min, and barely 1 at 240 min after the bolus injection.

(2) The skin ^{10}B concentrations are consistently higher than blood and normal liver (except for the earliest time point), approximately 1.7 times of liver. Therefore, it may be the primary target organ for determining limiting toxicity. Dose profiles for skin and hepatic colorectal metastases obtained using the FCB and the medium head phantom appear to confirm this, although accurate RBE values for the skin, liver and hepatic colorectal metastases could change the dose profiles obtained.

While the ^{10}B concentration ratio is lower than that seen in experimental brain tumor models, this is an encouraging result considering the constraints of the host environment, liver, which is a highly vascularized organ. However, with the high skin ^{10}B concentrations, to obtain a therapeutic ratio of greater than unity in liver represents a challenge for BNCT. Additional research should be conducted to derive the RBEs for the liver and the hepatic colorectal metastases. Once obtained, it will be possible to generate detailed dosimetric calculations and to determine the suitability of BNCT for the treatment of hepatic colorectal metastasis.

4..2 Recommendations for Future Work

From these experiments, a number of possibilities for future work have emerged. First, there might be experiments that could be conducted to resolve the question of the radiation damage target for BNCT. Currently, there are conflicting theories, although

some experiments have shown that vascular damage is probably the cause for necrosis in rat spinal cord, thereby suggesting that the vascular endothelial cells are the target cells rather than the CNS parenchyma[5]. From the pharmacokinetic results shown in this work, two sets of irradiation experiments can be done to distinguish between these two potential targets. For the first experiment, the irradiation would be administered shortly after the BPA-f injection, approximately 5 – 10 minutes. During this period, the blood/normal brain ^{10}B concentration ratio is very high, therefore, it CNS necrosis is observed, it could be concluded that the vascular endothelial cells are the primary target of BNCT radiation damage. For the second experiments, the animals would be irradiated 200 – 250 minutes after BPA-f injection. During this period, the normal brain ^{10}B concentration is approximately 2 – 4 times higher than the blood. If necrosis is observed, it would suggest that the CNS parenchyma is the primary target.

There are other experiments that can be conducted which would shed some light on the transport mechanism of BPA-f into tissues. First, there is the issue of spatial ^{10}B biodistribution in different brain structures. Amino acid studies have yielded data that suggest that there is differential influx for different amino acids in various brain structures[2]. Current experimental results also suggest that there is an elevated uptake of ^{10}B in the cerebellum and the intracranial nerves. Three types of experiments can be conducted to further investigate this issue. The first is to conduct similar animal studies using a large animal model with higher spatial resolution, such as dogs, to determine the^{10}B concentrations in these two structures. Secondly, the ^{10}B concentrations in these structures can be quantified using a microscopic technique, such as HRQAR. HRQAR can not only quantify ^{10}B in minute tissue samples, thus resolving the problem of inadequate spatial resolution in a small animal model, it can also be used to study the microdistribution of BPA-f in these brain structures, thus furthering our understanding of the dosimetry in these tissues. Thirdly, an experiment can be conducted in which a tracer quantity of ^{14}C labeled amino acid is infused and blood samples measured for amino acid concentrations, including competing amino acids. The samples could be thinly sectioned for quantitative autoradiography. By adequately taking into account the effects of protein incorporation and dilution to free amino acid pool, influx rates can be calculated[2]. The

principle of this approach is basically similar to that of the present research, but done at a higher spatial resolution.

Other research possibilities include manipulation of BPA-f influx using competing amino acids. The goal of such research would be to increase the amount of BPA-f transported into the tumor cells, thus elevating the ^{10}B concentration and further increasing the therapeutic ratio. Both phenylalanine and tyrosine are large neutral amino acids (LNAA) and are mainly transported into cells by the L-system. It has been shown in cell culture that BPA uptake is predominantly by the Na^+-independent L-system, and that BPA efflux from cells is also dependent on the L-system[5]. It has also been shown that the phenylalanine influx can be affected by the concentrations of other LNAA. By preloading the cells with tyrosine, the influx will increase, but if the system receives an infusion of leucine, the plasma concentration of tyrosine and phenylalanine are decreased by 40% and 45% respectively[6]. Once the transport mechanism of BPA-f is known, it will be possible to utilize the data gathered from the amino acid/protein metabolism research to manipulate the transport system in such as way as to increase BPA-f uptake. These experiments should first be conducted in cell culture, and then in small animal models such as the those used in this research. The new data, along with that presented in this research, can contribute to a more comprehensive pharmacokinetic model, in which the rate constants can be predicted based on the infusion scheme and the manipulations applied.

In addition to manipulating the amino acid concentrations in the system to preferentially increase BPA-f influx, another possibility is to increase the ^{10}B concentration in the blood. Neutral amino acids such as phenylalanine distribute readily into erythrocytes due to the presence of specific neutral amino acid transport systems on the red cell plasma membrane. Therefore, the blood cell amino acid red pool is important. The literature has suggested that once phenylalanine is absorbed by red blood cells, it is no longer available to be transported through the blood-brain barrier *in vivo* [7]. It has also been shown that human red blood cells have a specific amino transport system, the T-system[8], which is not present in most other cells. The T-system is a Na^+-independent system that shows significant transport of the aromatic amino acids tryptophan, tyrosine, and phenylalanine[8]. Since BPA-f is derived from phenylalanine,

but structurally similar to tyrosine, it is possible that BPA-f is also taken up into red blood cells by the T-system. Since the L-phenylalanine uptake by erythrocytes is saturable and nonconcentrative[9], it is conceivable that if the T-system in the red blood cells can be blocked, the concentration of phenylalanine and tyrosine in plasma will be elevated.

Better compartment models can also be derived if the transport mechanism and biochemical metabolism of BPA-f is understood. Numerous data are available on amino acid metabolism and protein turnover, which can provide useful data for modeling when the nature of BPA-f metabolism is known.

With respect to the issue of timing of the irradiation following BPA infusion, the present research shows that for different tumor cell lines, there may be a different optimal time frame. Therefore, more research should be focused on determining the pharmaokinetics of individual tumors by *in vivo* techniques, such as PET[3] and MRI. However, better resolution is a requirement for such an endeavor. From well vascularized animal tumors, it can be seen that the tumor uptake might be much higher than that observed in biopsies with necrotic regions. The study on the relationship between ^{10}B concentration and cellularity[1] also supports this observation. Therefore, better resolution than PET or MRI data will be needed to better predict the optimal irradiation time frame.

Finally, more animal studies could be conducted with the hepatic colorectal metastasis model to find the RBEs for liver, tumor, skin, and other gastrointestinal organs in the irradiation field. Dosimetic calculations could be done to further investigate the suitability of BNCT for this specific tumor. In addition, if this tumor shows some preferential uptake in a very challenging host environment, it is conceivable that other tumor types might also prove to have preferential BPA-f uptake compared to surrounding tissue. This possibility is well worth investigating.

4.3 References

1. Coderre, J.A., *et al.*, *Biodistribution of Boronophenylalanine in Patients with Glioblastoma Multiforme: Boron Concentration Correlates with Tumor Cellularity.* Radiation Research, 1998. **149**: p. 163-170.

2. Hawkins, R.A., A.M. Mans, and J.F. Biebuyck, *Amino Acid Supply to Individual Cerebral Structures in Awake and Anesthetized Rats.* American Journal of Physiology, 1982. **242**: p. E1-E11.

3. Imahori, Y., *et al.*, *Fluorine-18-labeled fluoroboronophenylalanine PET in patients with glioma.* Journal of Nuclear Medicine, 1998. **39**: p. 325-333.

4. Mishima, Y., *Selective thermal neutron capture therapy of cancer cells using their specific metabolic activities--melanoma as prototype.*, in *Cancer Neutron Capture Therapy*, Y. Mishima, Editor. 1996, Plenum Press: New York, N.Y. p. 1-26.

5. Morris, G.M., *et al.*, *Boron neutron capture irradiation of the rat spinal cord: histopathological evidence of a vascular-mediated pathogenesis.* Radiat Res, 1996. **146**(3): p. 313-320.

6. Alvestrand, A., *et al.*, *Influence of Leucine infusion on Intracellular Amino Acids in Humans.* European Journal of Clinical Investigation, 1990. **20**: p. 293-298.

7. Ellison, S. and W.M. Pardridge, *Red Cell Phenylalanine Is Not Available for Transport Through the Blood-Brain Barrier.* Neutrochemical Research, 1990. **15**(8): p. 769-772.

8. Harvey, C.M. and J.C. Ellory, *Identification of Amino Acid Transporters in the Red Blood Cell.* Methods in Enzymology, 1989. **173**: p. 122-160.

9. Pico, C., *et al.*, *Erythrocyte uptake kinetics and cell to plasma gradients of leucine and phenylalanine in fed and fasted rats.* Archives Internationales de Physiologie, de Biochimie et de Biophysique, 1993. **101**: p. 161-165.